GEOMICROBIOLOGY AND GEOCHEMISTRY OF FLUID FINE TAILINGS IN AN OIL SANDS END PIT LAKE

A Thesis Submitted to the College of

Graduate and Postdoctoral Studies

In Partial Fulfillment of the Requirements

For the Degree of Master of Science

In the Department of Geological Sciences

University of Saskatchewan

Saskatoon

By

SARAH BRETON RUDDERHAM

PERMISSION TO USE

In presenting this thesis in partial fulfillment of the requirement of a Postgraduate degree from the University of Saskatchewan, I agree that the Libraries of this University may make it freely available for inspection. I further agree that permission for copying of this thesis in any manner, in whole or in part, for scholarly purposes may be granted by the professor or professors who supervised my thesis work or, in their absence, by the Head of the Department of Geological Sciences or the Dean of the College of Graduate and Postdoctoral Studies. It is understood that any copying, publication or use of this thesis or parts thereof for financial gain shall not be allowed without my written permission. It is also understood that due recognition shall be given to me and to the University of Saskatchewan in any scholarly use which may be made of any material in my thesis.

Requests for permission to copy or to make other uses of materials in this thesis in whole or part should be addressed to:

Head of the Department of Geological Sciences
University of Saskatchewan
114 Science Place
Saskatoon, Saskatchewan S7N 5E2
Canada

Dean
College of Graduate and Postdoctoral Studies
University of Saskatchewan
116 Thorvaldson Building, 110 Science Place
Saskatoon, Saskatchewan S7N 5C9
Canada

ABSTRACT

End pit lakes are a proposed mine closure landscape for fluid fine tailings (FFT) in the Athabasca oil sands region of northern Alberta, Canada. Oil sands end pit lakes are created when FFT are transferred into a mined-out pit and capped with water. Base Mine Lake is the first full-scale demonstration end pit lake and is located at Syncrude Canada Limited's Mildred Lake mine. The geochemical development of Base Mine Lake has important implications for the viability of end pit lakes as a FFT reclamation strategy within the Alberta oil sands. The FFT is a source of several constituents that may negatively impact surface water quality through advective and diffusive transport mechanisms. This research examines relationships between microbiology and pore-water chemistry within FFT to inform predictions of long-term chemical mass loading from FFT to the water cap. Samples were collected from Base Mine Lake in 2016 and 2017, extending from 0.5 m above the tailings-water interface to 40 m below the interface. High-throughput amplicon sequencing of the 16S rRNA gene and a detailed analysis of FFT pore-water chemistry was conducted to identify the spatial distribution of microbial populations and associated geochemical gradients. The sequencing results identified microbes associated with various metabolisms, notably hydrocarbon degradation, sulfate reduction and methanogenesis. The importance of microbial metabolisms shifted with depth and the greatest potential for biogeochemical cycling was exhibited near the tailings-water interface. Pore-water pH decreased sharply below the interface from above 8.1 to below 7.8, and zones of nitrogen cycling, sulfate reduction and methane oxidation were identified within the upper 2 m of the FFT deposit. Biologically-driven reactions occurring in this zone can potentially reduce the flux of dissolved methane, ammonium and hydrogen sulfide across the interface, affecting mass flux calculations and estimations of long-term mass loading to the water cap. The microbial community in deeper FFT was dominated by hydrocarbon degraders, syntrophs and methanogens. Pore-water pH gradually decreased in this area to a minimum of 6.9 and dissolved methane concentrations remained above 30 mg L^{-1}. Microbial methane production is likely controlled by hydrocarbon degradation and long-term methanogenic rates and pathways will be largely dependent on the availability of substrates produced by syntrophic microbes. Findings from this study were also used to refine a conceptual model to better understand long-term mass loading of dissolved constituents.

ACKNOWLEDGEMENTS

I would first like to give a heartfelt thank you to my co-supervisors, Dr. Matt Lindsay and Dr. Joyce McBeth. I am so grateful for all the mentorship, support and encouragement you have given me over the course of my degree. You both have helped me grow as a writer and a scientist. Matt, the confidence you have in my abilities has kept me motivated throughout this process. Joyce, thank you for patiently entertaining all my questions; your kindness has meant so much to me. I would also like to thank my committee member Dr. Jim Hendry for his helpful comments throughout the progression of my degree and my external examiner Dr. Janet Hill for her constructive feedback.

A huge thank you to Noel Galuschik for being the glue that holds the field season together. Your ability to fit any assortment of objects into any size container will never cease to amaze me. Field work, lab work, writing, and life in general would be much harder (and not as fun) without you.

Thank you to the Mine Closure Research Team at Syncrude, especially Janna Lutz, Jessica Piercey and Mohamed Salem, for all your support with field sample collection and lab analysis. Field sample collection also could not have been completed without the assistance of ConeTec. Thank you to Dr. Peter Dunfield for your kind offer to help with my DNA sequencing and to Ilona Ruhl for welcoming me into your lab and taking the time to help me prepare and sequence my samples. Many thanks to Qingyang Liu for all your work processing the methane samples and to Matt Lindsay for processing the methane data. Thank you to Dr. Jing Chen and Fina Nelson for conducting pore-water analyses using the ICP-MS, ICP-OES and IC.

To the BML team - Daniel, Jared and Qingyang - it was comforting knowing there was always someone willing to chat about tough questions and share papers with. To all the people who made Saskatoon feel like home - Mattea, Carlo, Lawrence, Noel, Colton, James, Daniel, Scott, Aidan - I could not have asked for a better group of people to share these last two years with. Mattea, you were the best office mate – I wouldn't want to gab or power hour with anyone else.

Mom and Dad, your love and interest in everything I do has always meant so much to me. I wouldn't be where I am today without all your support along the way. Spencer, thank you for always being there for me, especially when I decided to move 3000 km away. Sarah D, you are the best cheerleader a girl could ask for.

TABLE OF CONTENTS

LIST OF TABLES

LIST OF FIGURES

LIST OF ABBREVIATIONS

ANME	anaerobic methanotrophic archaea
Anammox	anaerobic ammonium oxidation
BML	Base Mine Lake
BTEX	benzene, toluene, ethylbenzene, xylene
COSIA	Canada's Oil Sands Innovation Alliance
DNA	deoxyribonucleic acid
EC	electrical conductivity
Eh	reduction-oxidation potential
EPL	end pit lake
FFT	fluid fine tailings
HDPE	high density polyethylene
NMDS	non-metric multidimensional scaling
OTU	operational taxonomic unit
PCR	polymerase chain reaction
PES	polyesthersulfone
rRNA	ribosomal ribonucleic acid
SOI	sulfur oxidation intermediate
SRB	sulfate-reducing bacteria
TWI	tailings-water interface

CHAPTER 1: INTRODUCTION

The Alberta oil sands host one of the world's largest recoverable hydrocarbon reserves, containing an estimated 166 billion barrels of bitumen over three major areas in northern Alberta, Canada (Alberta Government, 2017). The Athabasca oil sands region is the largest deposit and contains relatively shallow deposits that can be recovered through surface mining techniques. Surface mining in this region has disturbed over 950 km^2 of land and the subsequent recovery of bitumen produces three tailings streams consisting of tailings sand, fluid fine tailings (FFT) and froth treatment tailings (Alberta Environment and Parks, 2017; Kasperski and Mikula, 2011). These tailings streams are composed of varying proportions of solids, water, residual bitumen and other organic compounds. The FFT stream is made up of a large proportion of clay- and silt-sized particles and initially has a low solids content of at least 2% (w/w) (COSIA, 2012). The estimated total volume of FFT held in the Athabasca oil sands region is nearly 1 billion m^3 and almost 20 000 m^3 of fine tailings can be generated daily (Alberta Environment and Parks, 2015; Small et al., 2015). Operators mining in this region are required to progressively reclaim and manage the volume of all fluid tailings and process water on site, as well as reclaim the land when their mining operations are over (Alberta Energy Regulator, 2017a).

Aquatic and terrestrial tailings reclamation strategies are actively being researched and can involve managing FFT through the addition of flocculants and coagulants, large-scale centrifugation and water capping (COSIA, 2012). Water capped tailings technology involves the creation of end pit lakes (EPLs), where FFT are transferred into a mined-out pit and capped with a mixture of fresh and process water. The long-term goal is for EPLs to become self-sustaining and functional aquatic ecosystems that can ultimately be incorporated into the surrounding watershed. The viability of EPLs as a successful reclamation strategy is therefore dependent on adequate surface water quality, which is strongly influenced by chemical mass loading from the underlying FFT. A main input of chemical constituents to the water cap is from the advective-dispersive flow of FFT pore water driven by tailings settlement (Dompierre et al., 2017). Over time, diffusion is also expected to become an important mass transport mechanism (Dompierre

and Barbour, 2016). These mass transport processes can potentially increase concentrations of dissolved constituents including sodium (Na), chloride (Cl), ammonium (NH_4^+), hydrogen sulfide ($\sum H_2S$) and methane (CH_4) in the water cap. Increased concentrations of these constituents will ultimately impact the development of an oxic water cap with acceptable water quality (Dompierre et al., 2016; Risacher et al., 2018).

A thorough understanding of the processes affecting FFT pore-water chemistry will aid in creating models used to predict long-term chemical mass loading and the geochemical development of EPLs. Base Mine Lake (BML) is the first full-scale demonstration EPL, established in December 2012 and located at Syncrude Canada's Mildred Lake mine. Analysis of FFT biogeochemistry within BML will provide valuable information related to the viability of EPLs as an aquatic reclamation strategy in the Athabasca oil sands region. A conceptual model for FFT biogeochemistry in BML was created based on literature published from past field and laboratory studies (Figure 1-1). This conceptual model can be used to identify biotic and abiotic processes that influence FFT pore-water chemistry and predict how these processes can impact long-term mass loading of salts, NH_4^+, $\sum H_2S$ and CH_4 to the water cap. The model establishes that microbially-driven reactions have both direct and indirect influences on FFT pore-water chemistry and FFT consolidation. Specifically, anaerobic microbial processes can decrease pore-water pH, which promotes the dissolution of carbonate minerals and results in increased concentrations of bicarbonate (HCO_3^-), calcium (Ca^{2+}) and magnesium (Mg^{2+}) in FFT pore water (Figure 1-1). Exchange of divalent cations for Na^+ at the clay mineral surface reduces the thickness of the electrical double layer, resulting in enhanced FFT consolidation (Dompierre et al., 2016; Siddique et al., 2014a). Microbially-driven redox reactions also affect the concentrations of dissolved iron (Fe), sulfur (S) and carbon (C) species, and these geochemical cycles can be coupled to one another (Figure 1-1). Sulfate reduction occurring in FFT produces $\sum H_2S$ and the concentration of this constituent can be controlled by precipitation of Fe(II)-sulfide phases (Dompierre et al., 2016; Stasik et al., 2014). Methane production, or methanogenesis, also occurs in FFT from organic C degradation and gas bubbles form when concentrations reach saturation (Siddique et al., 2007; Stasik and Wendt-Potthoff, 2016).

Studies related to oil sands tailings ponds have identified the presence of diverse microbial communities that drive the biogeochemical cycles of nitrogen (N), Fe, S and C within FFT (Foght

et al., 2017; Penner and Foght, 2010; Stasik et al., 2014). An examination of microbial community structure in an EPL setting could verify the assumptions made in the existing conceptual model that specific microbes are catalyzing the established redox reactions. A microbiological analysis could also identify microbes capable of catalyzing reactions that were not considered in the initial model. An examination of N biogeochemistry is also important to consider in the conceptual model because NH_4^+ concentrations can be elevated in FFT pore water and mass loading of this constituent can negatively impact the cap water quality. Finally, an investigation of depth-dependent changes in FFT biogeochemistry would further refine the conceptual model. Depth-related information is important for predicting how concentrations of dissolved N, Fe, S and C species will be altered throughout the FFT deposit. Specifically, this information would allow for better understanding and predictions of NH_4^+, $\sum H_2S$ and $CH_{4(aq)}$ mass loading to the water cap.

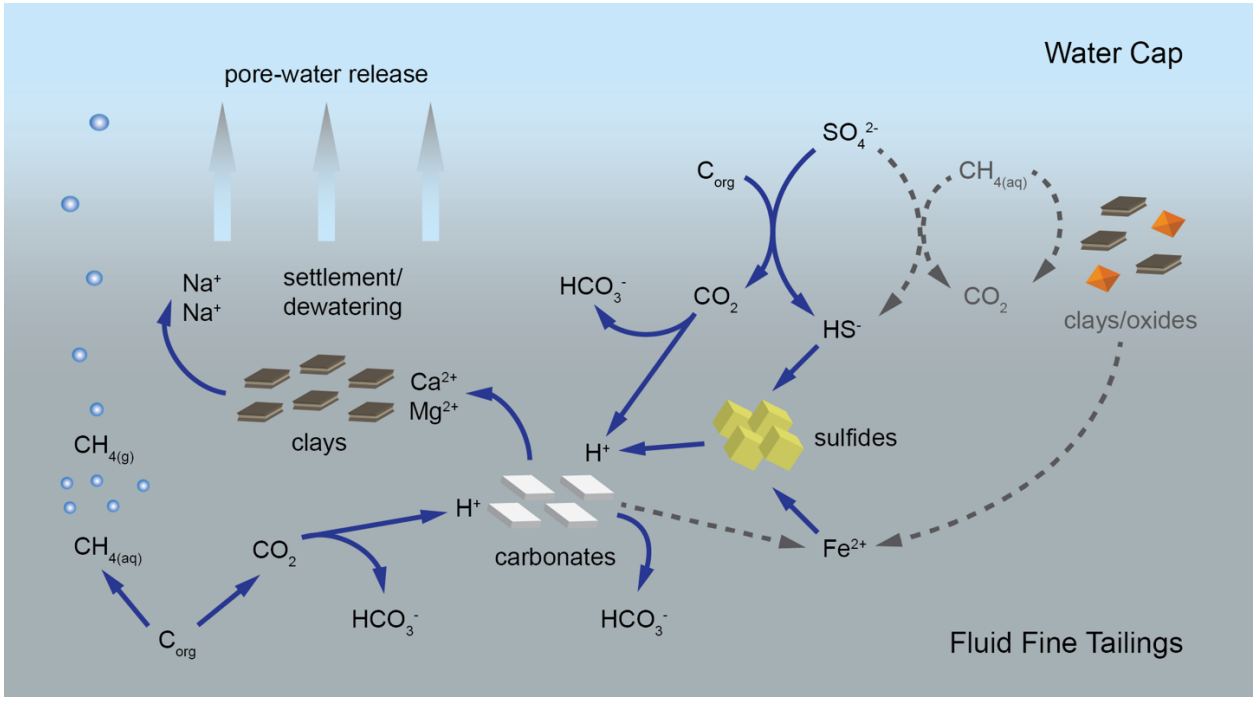

Figure 1-1: Current conceptual model for FFT biogeochemistry. The solid lines represent processes reported in the literature and the dotted lines represent processes thought to occur based on current knowledge.

1.1 Research Objectives

The overall goal of this research is to develop an understanding of the relationships between FFT microbiology and pore-water chemistry in BML. Microbes catalyze the redox reactions occurring in FFT and examination of these relationships can offer unique insight into biogeochemical processes controlling pore-water chemistry. These findings will support the development of a conceptual model for FFT biogeochemistry and inform predictions of long-term chemical mass loading from FFT to the water cap.

The specific objectives of this study are:

i) determine the spatial distribution of microbial populations and associated geochemical gradients in the BML tailings deposit;
ii) identify how microbial processes can impact water chemistry and mass-transfer reactions across the tailings-water interface; and
iii) refine the conceptual model for FFT biogeochemistry within BML.

CHAPTER 2: LITERATURE REVIEW

2.1 Tailings Management in the Alberta Oil Sands

Oil sands deposits in northern Alberta, Canada contain an estimated 166 billion barrels of recoverable bitumen reserves split among the Athabasca, Cold Lake and Peace River deposits (Alberta Government, 2017). These deposits extend over an 142 000 km^2 area where surface mineable bitumen is hosted in sands and sandstones of the Cretaceous McMurray formation (Chalaturnyk et al., 2002). Bitumen is a heavy and viscous form of crude oil that can be recovered using in situ or surface mining techniques. In situ techniques are used to recover deposits deeper underground, typically greater than 200 m below the surface, and can be used to recover approximately 80% of the oil sand reserves (Government of Alberta, 2009). Surface mining can recover deposits up to 80 m below surface and can only be used in a 4 800 km^2 area within the Athabasca oil sands region. Bitumen recovery from surface-mined ore is greater than in situ methods, however it results in the surface disturbance of Alberta's boreal forest (Government of Alberta, 2009; Kasperski and Mikula, 2011). Surface mining involves transporting mined oil sand to a processing facility where hot water and process aids (e.g., sodium hydroxide, sodium citrate, diluents) are used to separate bitumen from the sand- and clay-sized particles (Small et al., 2015). A by-product from this extraction process is mixture of solids (particle size generally <44 μm) and oil sands process-affected water, referred to as FFT. These tailings have low settlement rates and elevated concentrations of salts, naphthenic acids, unrecovered bitumen and residual diluent (Allen, 2008; Kasperski and Mikula, 2011). Substantial FFT volumes are produced daily and currently these tailings are stored on site due to strict regulations for water release to the environment (Alberta Government, 2015). Typically, FFT are stored in large oil sands tailings ponds where self-weight consolidation drives the release of pore water over time and the expressed pore water is recycled back into the bitumen extraction process. The FFT settle to 20% (w/w) solids within a few weeks, however it can take three to five years to reach 30% (w/w) solids, at which point they are often referred to as mature fine tailings (Allen, 2008; Kasperski and Mikula, 2011). This slow settlement and dewatering poses as a major challenge for managing the nearly

1 billion m^3 of FFT stored in tailings ponds covering an 88 km^2 region in the Athabasca oil sands (White and Liber, 2018).

Oil sands operators are required to progressively treat and reclaim tailings during mining to prevent increases in FFT inventories stored in tailings ponds (Alberta Energy Regulator, 2017a). The disturbed land must also be reclaimed to equivalent pre-mining land use once mining operations are over. Process water and FFT therefore need to be integrated back into the landscape through various aquatic and terrestrial ecosystems. Associated reclamation technologies are in various stages of development and their long-term viability is being actively researched (Dompierre et al., 2016; Reid and Warren, 2016). Some terrestrial reclamation technologies involve creating artificial landscapes using composite tailings and centrifuged fine tailings. These methods typically require FFT to be amended with a coagulant, such as gypsum, to increase its bearing capacity and shear strength before a soil cover can be placed over it (Kasperski and Mikula, 2011). Aquatic reclamation includes the creation of EPLs, also referred to as water-capped tailings technology, where FFT are transferred to a mined-out pit and capped with a combination of fresh and process water. This method does not require chemical amendment, although some operators may use flocculants and coagulants to accelerate tailings dewatering (Alberta Energy Regulator, 2017b; COSIA, 2012). The use of readily available fill material also allows for a cost-effective reclamation strategy and can better accommodate daily FFT production. However, success of EPLs as a tailings management strategy is dependent on the long-term evolution of cap water quality (COSIA, 2012). In addition to limited chemical and toxicological risk, the water cap layer will require sufficient oxygen (O_2) concentrations to sustain a biological community (White and Liber, 2018). Recent research has identified that the main input of chemical constituents to the water cap during early stage development is from advective-dispersive transport of FFT pore water driven by tailings settlement (Dompierre et al., 2017). However, few studies have analyzed the factors that influence FFT pore-water chemistry in an EPL (Dompierre et al., 2016). The potential for microbes to impact the mass transfer of chemical constituents across the tailings-water interface (TWI) has not yet been examined.

Microbes influence the oxidation state of redox sensitive elements in a variety of natural and anthropogenic environments (Bethke et al., 2011). Past studies identified the presence of diverse microbial communities in FFT and composite tailings deposits that are capable of

influencing the biogeochemical cycles of N, Fe, S and C (Foght et al., 2017; Penner and Foght, 2010; Warren et al., 2016). The chemical speciation and abundance of these elements are of interest in assessing EPL viability because they can impact the geochemical development of the water cap. For instance, fluxes of dissolved NH_4^+, $\sum H_2S$ and CH_4 across the TWI can consume O_2 and impede the development of an oxic water cap (Risacher et al., 2018). Fluxes of dissolved salts, including sulfate (SO_4), and elevated concentrations of NH_4^+ can also negatively impact water cap quality. Research into oil sands EPLs has only recently been initiated and the role of microbes in their biogeochemical development is poorly constrained. Key knowledge gaps include (i) the relationship between microbial communities and FFT pore-water chemistry and (ii) the impact of this relationship on the distribution and abundance of dissolved constituents across the TWI. The redox processes of interest are commonly observed in marine and freshwater sediments, as well as tailings ponds, where labile organic matter is degraded in the absence of O_2. An understanding of these processes in O_2-limited environments is important to interpret how FFT biogeochemistry will evolve over time and affect the development of a self-sustaining EPL.

2.2 Redox Geochemistry and Microbiology

The biogeochemical cycles of many major elements are driven by microbially-mediated redox reactions. These reactions require the transfer of electrons from a reduced electron donor species to an oxidized electron acceptor species (Champ et al., 1979). Common electron donors for microbial metabolic processes in aqueous environments include low molecular weight carbon molecules, such as acetate (CH_3COO^-), CH_4, lactate, and some n-alkanes, as well as hydrogen (H_2). Common electron acceptors include O_2, nitrate (NO_3), Fe(III) and SO_4 (Bethke et al., 2011). Microbes live by harnessing the energy released when they catalyze the transfer of these electrons. Microbes that can catalyze reactions that yield more energy would therefore have a thermodynamic advantage and competitively exclude other microbes in the system (Chapelle and Lovley, 1992). The redox ladder, also known as the thermodynamic ladder, predicts the order that redox reactions will occur in the environment. It is based on thermodynamic principles and suggests that reactions yielding the highest free energy, or most negative ΔG value, will occur first and reactions yielding the lowest free energy will occur last (Bethke et al., 2011). Based on this principle, the order of major redox processes in the environment would proceed as aerobic respiration first, followed by

anaerobic respiration processes, including NO_3 reduction, manganese (Mn) reduction, Fe(III) reduction, SO_4 reduction and methanogenesis (Table 2-1).

Table 2-1: Free energy associated with electron-donating and electron-accepting half reactions in O_2-limited environments. The ΔG values were derived using the parameters T=25°C and pH=7 (Bethke et al., 2011).

Electron-Donating Half Reactions		**ΔG (kJ mol^{-1})**
Acetotrophy	$CH_3COO^- + 4H_2O \rightarrow 2HCO_3^- + 9H^+ + 8e^-$	-216
Hydrogentrophy	$4H_{2(aq)} \rightarrow 8H^+ + 8e^-$	-185
Electron-Accepting Half Reactions		
Nitrate reduction	$8e^- + NO_3^- + 10H^+ \rightarrow NH_4^+ + 3H_2O$	-297
Iron reduction	$8e^- + 8Fe(OH)_3 + 24H^+ \rightarrow 8Fe^{2+} + 24H_2O$	-4 to 96
Sulfate reduction	$8e^- + SO_4^{2-} + 9H^+ \rightarrow HS^- + 4H_2O$	150
Methanogenesis	$8e^- + HCO_3^- + 9H^+ \rightarrow CH_{4(aq)} + 3H_2O$	184

This sequence of reactions does not always proceed as predicted, and some reactions may occur simultaneously due to environmental and physiological factors (Bethke et al., 2011). When a microbe catalyzes a redox reaction, a fraction of the energy released is harnessed to produce adenosine triphosphate, a molecule used to store energy for cell functions. The remaining usable energy available in the environment can be used to drive reactions for cell metabolism (Bethke et al., 2011). Changes in pH can alter the usable energy for redox reactions that produce or consume protons. This is because a proton motive force is created during the electron transport chain and changes in pH directly affect the proton gradient and can prevent it from being generated (Jin and Kirk, 2018). Microbes capable of Fe(III) reduction with goethite have a strong thermodynamic advantage when pH is below 6.5, whereas there is no usable energy to drive goethite reduction in alkaline environments (Bethke et al., 2011; Flynn et al., 2014). Additionally, methanogens have a similar usable energy to Fe(III) reducers and SO_4 reducers in near-neutral environments because they trap less energy per mole of electron donor consumed (Bethke et al., 2011). The dominance of one metabolism over another can be attributed to their growth rates, where SO_4 reducers are able to reproduce at a faster rate than methanogens (Bethke et al., 2008).

Redox dynamics can also be influenced by the concentration and bioavailability of electron donors, acceptors and reaction products. An abundance of SO_4 increases the usable energy for SO_4 reducers and can result in their ability to dominate over methanogens when competing for the same carbon source, such as CH_3COO^- (Bethke et al., 2011). However, SO_4 reducers and methanogens can also coexist when they consume different electron donors (Mitterer, 2010; Stasik and Wendt-Potthoff, 2016). Furthermore, Fe(III) reducers and SO_4 reducers can engage in a mutualistic relationship to limit the accumulation of Fe(II) and $\sum H_2S$ that would inhibit their growth. In a bioreactor experiment, the reaction products were produced in approximate 1:1 mole ratios, which promoted the precipitation of $FeS_{(s)}$ and the subsequent removal of these products from solution (Bethke et al., 2011).

The progression of redox reactions that will occur in an O_2-limited environment can be attributed to thermodynamics, environmental chemistry and microbial physiology. While the water cap of EPLs will likely support some reactions with O_2 as the electron acceptor (Risacher et al., 2018), the underlying tailings are likely to be dominated by anaerobic redox reactions (Dompierre et al., 2016). The potential for N, Fe, S and C cycling in FFT deposits has been established for oil sands tailings ponds (Foght et al., 2017). A greater understanding of the relationship between microbial community structure and observed geochemical gradients in EPL settings can provide insight into the redox dynamics for these reclamation scenarios. These relationships can help to constrain which redox processes are occurring in the FFT and how they can affect long-term mass loading of dissolvent chemical constituents across the TWI.

2.3 Nitrogen Cycling

Nitrogen is commonly found in aqueous environments as NO_3 and nitrite (NO_2) under oxic conditions, and ammonia (NH_3) under anoxic conditions. The NH_4^+ ion dominates aqueous NH_3 speciation at pH below 9.3, which is consistent with circumneutral pH pore waters in FFT deposits (Dompierre et al., 2016). Concentrations of NO_2 and NO_3 are generally below detection limits in FFT pore water, whereas NH_4^+ concentrations above 10 mg L^{-1} have been documented (Dompierre et al., 2016; Stasik et al., 2014). The flux of NH_4^+ to the water cap is of concern in EPLs because it can negatively impact water quality and microbial nitrification can consume O_2. Production and consumption reactions involving NH_4^+ are important to constrain; however, detailed knowledge of N cycling in oil sands tailings ponds and EPLs is not well defined.

Nitrification (Equation 2.1) was recently identified as an active and important process affecting water cap O_2 concentrations within a pilot EPL (Risacher et al., 2018).

$$NH_4^+ + 2O_2 \rightarrow NO_3^- + H_2O + 2H^+ \quad (2.1)$$

Nitrification was not previously documented as a major process occurring in oil sands tailings ponds, potentially due to high concentrations of naphthenic acids inhibiting the activity of nitrifying microbes (Misiti et al., 2013). The emergence of this active process in EPLs demonstrates the need for biogeochemical studies in reclamation scenarios, since studies of tailings pond biogeochemistry are unlikely to be directly applicable to long-term EPL biogeochemistry. A study examining the initial geochemical characteristics of FFT in a pilot EPL identified that average NH_4^+ concentrations were 10 mg L^{-1} and minimum concentrations occurred at the TWI (Dompierre et al., 2016). The potential role of anaerobic ammonium oxidation (anammox) on controlling NH_4^+ concentrations below the TWI is not known. Anammox is a microbial process where NH_4^+ is anaerobically oxidized to nitrogen gas using NO_2 as the electron acceptor (Equation 2.2) and it is well documented in marine and freshwater sediments (Devol, 2015; Schubert et al., 2006). All known anammox bacteria belong to the phylum *Planctomycetes* and are further classified into five *Candidatus* genera: *Candidatus Brocadia, Candidatus Kuenenia, Candidatus Scalindua, Candidatus Anammoxoglobus* and *Candidatus Jettenia* (Wenk et al., 2013). The occurrence of anammox in EPLs could reduce NH_4^+ mass loading to the water cap and result in a loss of total N from the system via nitrogen gas production. Ammonium oxidation via anammox processes can also occur using electron acceptors coupled with other biogeochemical cycles; for example, NH_4^+ oxidation coupled to reduction of Fe(III) (Equation 2.3) (Bao and Li, 2017).

$$NH_4^+ + NO_2^- \rightarrow N_2 + 2H_2O \quad (2.2)$$

$$3Fe(OH)_3 + 5H^+ + NH_4^+ \rightarrow 3Fe^{2+} + 9H_2O + 0.5N_2 \quad (2.3)$$

A comprehensive depth profile of N species in EPL tailings deposits is needed to understand and predict long-term mass fluxes, as well as constrain the N mass balance. An examination of microbial communities present in FFT can provide further insight into potential production and consumption reactions relevant to EPL environments. Previous enumeration studies identified NO_3-reducing microbes in process-affected water and FFT and anaerobic denitrifying bacteria were identified in FFT in various tailings ponds in the Athabasca oil sands

region (Fedorak et al., 2002). A study examining 16S ribosomal ribonucleic acid (rRNA) gene clone libraries in fine tailings further identified the NO_3-reducing genus *Thaurea* (Penner and Foght, 2010). However, the metabolic roles of these microbes in oil sands tailings ponds and EPLs are poorly defined.

2.4 Iron Reduction

Dissolved Fe is found in aqueous systems as oxidized ferric iron (Fe(III)) or reduced ferrous iron (Fe(II)) and its speciation is highly pH-dependent. Total dissolved Fe concentrations in FFT pore water are likely dominated by Fe(II). This is because Fe(III) (hydr)oxides are rarely soluble at circumneutral pH values and FFT pore-water pH generally ranges from 7.0 to 8.5 (Foght et al., 2017; Postma and Jakobsen, 1996). Iron reduction in EPLs is an important process to consider in terms of water quality because Fe(II) can react with reduced S species, resulting in $FeS_{(s)}$ mineral precipitation (Equation 2.4). This reaction can control the $\sum H_2S$ flux across the TWI and therefore decrease the concentration of an O_2-consuming constituent that can be harmful to aquatic life in large concentrations. Field and laboratory studies related to FFT pore-water chemistry in tailings ponds identified the occurrence of $FeS_{(s)}$ mineral precipitation over a narrow depth range below the TWI (Chen et al., 2013; Siddique et al., 2014b; Stasik et al., 2014).

$$Fe^{2+} + HS^- \rightarrow FeS_{(s)} + H^+ \quad (2.4)$$

Dissolved Fe concentrations measured in an oil sands tailings pond and pilot EPL containing FFT ranged from less than 0.1 to 0.6 mg L^{-1} and increased concentrations were observed within the first 3 m below the TWI (Dompierre et al., 2016; Stasik et al., 2014). The Fe(III) (hydr)oxides and structural Fe(III) present in clay minerals can potentially be used as electron acceptors for iron-reducing bacteria (Dong et al., 2003; Penner and Foght, 2010). Enumeration studies have identified that cell numbers for iron-reducing bacteria in tailings ponds increase below the TWI (Fedorak et al., 2002; Stasik et al., 2014). Clone libraries constructed from the 16S rRNA gene also identified the presence of *Rhodoferax ferrireducens* in fine tailings and this microbe comprised between 4 and 20% of the libraries (Penner and Foght, 2010). However, few studies have examined the spatial distribution of iron-reducing bacteria, including *Rhodoferax*, and observed geochemical gradients in tailings ponds or EPLs. The spatial distribution and taxonomic

diversity of iron-reducing bacteria in these environments needs to be examined because Fe reduction in EPLs has important implications for long-term water cap quality.

2.5 Sulfur Cycling

2.5.1 Sulfate Reduction

Sulfur exists in the environment in multiple oxidation states and is most common as oxidized SO_4 and reduced $\sum H_2S$. Oil sands process water typically contains elevated SO_4 concentrations and values commonly range between 200 and 300 mg L^{-1} (Allen, 2008). Increased SO_4 concentrations in EPL water caps can impede the development of a self-sustaining biological community and can hinder the ability to discharge the cap water to the surrounding watershed. Studies on S cycling in a pilot EPL and tailings pond containing FFT identified that water cap SO_4 concentrations decrease sharply below the TWI due to microbial SO_4 reduction (Dompierre et al., 2016; Stasik et al., 2014). This process was also identified in an pond containing tailings routinely treated with gypsum ($CaSO_4 \bullet H_2O$) (Ramos-Padrón et al., 2011). Sulfate reduction in tailings environments is a biologically-driven reaction where SO_4 is completely reduced to $\sum H_2S$ through the activity of sulfate-reducing bacteria (SRB). These anaerobic microbes can consume various labile organic acids or H_2 as electron donors and use SO_4 as the terminal electron acceptor (Equation 2.5). Sulfide speciation in FFT pore water is likely dominated by HS^- because the pK_{a1} for H_2S is 7.0 and FFT pore-water pH is typically above that value (Foght et al., 2017).

$$SO_4^{2-} + 4HCOO^- + H^+ \rightarrow HS^- + 4HCO_3^- \quad (2.5)$$

Microbes capable of reducing SO_4 and other S compounds are minor members of the bacterial water cap community and can comprise a large proportion of the bacterial FFT community (Penner and Foght, 2010; Ramos-Padrón et al., 2011). These microbes are typically classified to the class *Deltaproteobacteria* and include *Desulfocapsa, Desulfurivibrio, Desulfatibacillum* and *Desulfobulbaceae* (Foght et al., 2017). Although it is established that a distinct zone of SO_4 reduction occurs below the TWI, most biogeochemical studies examine this process using only a few bulk samples. An examination of the relationship between microbial community structure and pore-water chemistry at a high spatial resolution below the TWI will offer insight into biogeochemical processes controlling S cycling.

A laboratory study recently demonstrated that SO_4 reduction can occur throughout the FFT deposit in tailings ponds, depending on the availability and concentration of electron donors and acceptors (Stasik and Wendt-Potthoff, 2016). The fate and occurrence of $\sum H_2S$ in EPLs is important to constrain because $\sum H_2S$ is an O_2-consuming constituent and can be harmful to aquatic life (Risacher et al., 2018). Secondary sulfide precipitation reactions (Equation 2.4) can occur in the FFT deposit at depths where dissolved Fe(II) is present and these reactions can decrease $\sum H_2S$ mass loading to the water cap (Foght et al., 2017). Dissolved $\sum H_2S$ that is not consumed by $FeS_{(s)}$ precipitation will likely be oxidized to SO_4 in the water cap through chemical or biological mechanisms. Dissolved $\sum H_2S$ also has the potential to remain in the water cap if O_2 is not present. A comprehensive examination of depth-dependent changes in FFT pore-water chemistry and microbial community structure will provide a greater understanding towards the abundance and distribution of SO_4 and $\sum H_2S$ species in EPL settings.

2.5.2 Sulfur Oxidation Intermediates

Sulfur oxidation intermediates (SOIs) are S compounds with intermediate oxidation states and can be formed through chemical and biological redox processes. The stepwise oxidation of $\sum H_2S$ to SO_4 can be a source of various SOIs in anoxic sediments (Zopfi et al., 2004). These species can include sulfite (SO_3^{2-}), thiosulfate ($S_2O_3^{2-}$), elemental sulfur (S^0) and polythionates ($S_nO_6^{2-}$). Chemical $\sum H_2S$ oxidation can occur in anoxic sediments with Mn(IV) and Fe(III) oxides as electron acceptors, typically yielding elemental S (Equation 2.6) (Zopfi et al., 2004). Dissimilatory metal-reducing bacteria can then respire elemental S directly (Flynn et al., 2014). For example, the elemental S-respiring microbe *Desulfuromonas* is found in FFT samples (Ramos-Padrón et al., 2011; Siddique et al., 2011).

$$2FeOOH + HS^- + 5H^+ \rightarrow 2Fe^{2+} + S^0 + 4H_2O \quad (2.6)$$

The SOIs produced in anoxic sediments can eventually be oxidized completely to SO_4 or reduced back to $\sum H_2S$. Disproportionation reactions can also occur, where an SOI is both oxidized and reduced (Zopfi et al., 2004). For instance, *Desulfocapsa* can disproportionate elemental S, producing SO_4 and $\sum H_2S$ (Equation 2.7). This microbe has been identified in FFT and gypsum-amended tailings, however its metabolic role in these tailings materials is not well defined (Penner and Foght, 2010; Ramos-Padrón et al., 2011).

$$4S^0 + 4H_2O \rightarrow SO_4^{2-} + 3HS^- + 5H^+ \quad (2.7)$$

Research has demonstrated that the production and consumption of SOIs can drive the S cycle in anoxic marine and freshwater sediments (Findlay and Kamyshny, 2017; Zopfi et al., 2004). However, the occurrence and role of SOIs in oil sands tailings environments has yet to be examined. The importance of SOIs as key intermediates should be studied, considering they can be used as terminal electron acceptors for microbes found in oil sands tailings deposits. Understanding the role of SOIs in an EPL environment can help to better constrain the S mass balance and predict the fate of SO_4 and $\sum H_2S$ in the system.

2.6 Methanogenesis

Methanogenesis is a microbial process resulting in the production of CH_4 and it is an active process occurring in FFT. Methanogenesis has been linked to increased consolidation rates in FFT, which is important in context of minimizing the large FFT volumes stored in the Athabasca oil sands (Siddique et al., 2014a). However, microbially-driven $CH_{(aq)}$ oxidation can deplete O_2 concentrations in an EPL water cap (Risacher et al., 2018). Methane ebullition from the underlying FFT can also increase emissions of a greenhouse gas to the atmosphere (Holowenko et al., 2000). Methanogens are the microbes responsible for CH_4 production and all known methanogens are strictly anaerobic and belong to the archaeal domain. Methanogens are limited to the utilization of CH_3COO^-, carbon dioxide (CO_2) and methyl-group containing compounds for their metabolism (Liu and Whitman, 2008). Their proliferation in tailings environments is therefore largely dependent on the breakdown of other carbon sources by syntrophic microbes. For example, syntrophs can ferment fatty acids, aromatics and alcohols to CH_3COO^-, CO_2 and H_2. In turn, some methanogens consume H_2, which maintains a low partial pressure and allows the reactions that syntrophs catalyze to remain thermodynamically favourable (Liu and Whitman, 2008). Methanogenesis typically occurs through acetoclastic (Equation 2.8) or hydrogenotrophic (Equation 2.9) pathways in the environment (Bethke et al., 2011).

$$CH_3COO^- + H_2O \rightarrow CH_4 + HCO_3^- \quad (2.8)$$

$$CO_2 + 4H_2 \rightarrow CH_4 + 2H_2O \quad (2.9)$$

The main substrate that sustains methanogenesis in oil sands tailings ponds is residual diluent that is pumped into tailings ponds with fresh FFT (Siddique et al., 2007). Naphtha is used as a diluent during bitumen extraction by some oil sands operators, including Syncrude Canada Ltd. This diluent is a mixture of low molecular weight hydrocarbons, including *n*-alkanes and BTEX (benzene, toluene, ethylbenzene, xylene) compounds. Degradation of these compounds can be carried out by various microbes that break down the substrates to CH_3COO^-, H_2 and CO_2, which can be consumed by acteoclastic or hydrogenotrophic methanogens (Foght et al., 2017). For instance, the syntrophic deltaproteobacterial genera *Syntrophus* and *Smithella* can anaerobically degrade alkanes to CH_3COO^-, which can then be consumed by acetoclastic methanogens belonging to the order *Methanosarcinales* (Siddique et al., 2012). It is also proposed that some SRB oxidize CH_3COO^- to CO_2, which can be subsequently converted to CH_4 by hydrogenotrophic methanogens belonging to the order *Methanomicrobiales* (Stasik and Wendt-Potthoff, 2016).

Various laboratory studies have established the potential for CH_4 production from the biodegradation of naphtha components (Siddique et al., 2006, 2007, 2011). Microbes indigenous to fine tailings prefer to metabolize short-chain *n*-alkanes (C_6-C_{10}), toluene, xylenes and long-chain *n*-alkanes (C_{14}-C_{18}). The dominant methanogenic pathway occurring in laboratory enrichment cultures was dependent on the type and abundance of alkanes, BTEX and other naphtha compounds present (Siddique et al., 2012). Additionally, 16S rRNA gene sequencing studies identified archaeal sequences in fine tailings samples that classified to both hydrogenotrophic (*Methanoregula* and *Methanolinea*) and acteoclastic (*Methanosaeta*) methanogens (Foght et al., 2017; Siddique et al., 2014b). Most oil sands CH_4 biogeochemical studies have relied on laboratory enrichment cultures and bulk samples (Foght et al., 2017). A field examination of depth-dependent $CH_{4(aq)}$ concentrations, solubility, and archaeal community structure can provide insight into long-term methanogenic rates and pathways in EPLs containing tailings treated with naphtha.

Finally, a large focus of oil sands research is directed toward the relationship between SO_4 reduction and methanogenesis. Results from laboratory experiments have suggested that methanogenesis in tailings ponds can be inhibited by SO_4 reduction due to the low free energy yield of methanogens compared to SRB (Holowenko et al., 2000; Ramos-Padrón et al., 2011). However, SO_4-reducing and methanogenic activity can be observed concurrently when the concentration of carbon sources is high or the substrates are used non-competitively (Mitterer,

2010; Stasik et al., 2014). Results from microcosm experiments have further demonstrated that labile carbon substrate addition can cause a significant increase in simultaneous SO_4 reduction and methanogenesis (Stasik and Wendt-Potthoff, 2014, 2016). Available carbon sources vary depending on the age and depth of tailings in EPLs and tailings ponds. Knowledge of the environmental parameters required to stimulate methanogenic activity and how various microbial communities interact with each other is relevant when planning long-term reclamation strategies. Research further examining the relationship between overall microbial community structure and associated geochemistry can aid in developing a conceptual model for EPL tailings biogeochemistry.

2.7 Methane Oxidation

Dissolved CH_4 produced in tailings deposits could be oxidized by microbes known as methanotrophs as it moves from underlying FFT towards the water cap. Microbes capable of oxidizing $CH_{4(aq)}$ include aerobic methanotrophic bacteria and anaerobic methanotrophic archaea (ANME) (Foght et al., 2017). Aerobic methanotrophs require O_2 (Equation 2.10) and are present in the water cap of oil sands tailings ponds containing naphtha-treated FFT. The microbes are typically classified to the class *Gammaproteobacteria* and can include the genera *Methylocaldum* and *Methylomonas* (Saidi-Mehrabad et al., 2013). A recent geochemical study of a pilot EPL measured dissolved CH_4 concentrations of up to 150 µM at the TWI and near-zero at the surface, suggesting consumption by methanotrophs (Goad, 2017; Risacher et al., 2018). The study further indicated that aerobic methanotrophs can outcompete nitrifying microbes, demonstrating that CH_4 oxidation in the water cap of EPLs is a dominant O_2-consuming process.

$$CH_4 + 2O_2 \rightarrow CO_2 + 2H_2O \quad (2.10)$$

Anaerobic CH_4 oxidation in tailings ponds and EPLs could greatly decrease dissolved CH_4 fluxes across the TWI. This process has not been documented in oil sands environments, but does occur in freshwater and marine sediments. Known ANME are capable of consuming SO_4 (Equation 2.11), Fe(III), Mn(IV), NO_2 (Equation 2.12) and NO_3 as electron acceptors (Beal et al., 2009; Luo et al., 2018).

$$CH_4 + SO_4^{2-} \rightarrow HCO_3^- + HS^- + H_2O \quad (2.11)$$

$$3CH_4 + 8NO_2^- + 8H^+ \rightarrow 3CO_2 + 4N_2 + 10H_2O \quad (2.12)$$

Anaerobic CH_4 oxidation coupled to SO_4 reduction is common in marine sediments by microbes classified to ANME-1 and ANME-2 groups (Yanagawa et al., 2011). Sub-groups within ANME are thought to contain microbes capable of utilizing NO_3, Fe(III) and Mn(IV) (Beal et al., 2009). A bacterial organism belonging to the NC10 phylum can also couple CH_4 oxidation with NO_3 or NO_2 reduction (Ettwig et al., 2010). An analysis of microbial community structure in EPL tailings could indicate the presence of anaerobic CH_4-oxidizing microbes and the potential for this advantageous reaction to occur.

CHAPTER 3: METHODOLOGY

3.1 Site Description

Base Mine Lake is located approximately 40 km north of Fort McMurray, Alberta, Canada at Syncrude Canada Limited's Mildred Lake mine (Figure 3-1). The site makes up a portion of the original mine pit and was an active tailings pond referred to as West-In Pit until the end of 2012. Deposition of FFT to West-In Pit began in 1994 and was pumped from the Mildred Lake Settling Basin into the pit. The FFT from the Mildred Lake Settling Basin contains residual naphtha and is not amended with gypsum. During filling, a water cap ranging in depth between 3 and 5 m was present because of FFT dewatering. The FFT deposition ceased once the site was commissioned as an EPL in December 2012 and the name changed to BML. During that time, the maximum FFT thickness was approximately 45 m and the total volume of FFT was approximately 186 Mm^3. Once commissioned as an EPL, a mixture of fresh and process water was added to the cap to increase the water surface elevation to approximately 308.5 m above sea level. Three permanent sampling and measurement platforms were established in 2013 along a southwest to northeast transect of BML (Figure 3-2). The average water cap depth increased from approximately 8.5 m in 2015 to approximately 10 m in 2017 due to FFT settlement and dewatering. Currently, cap water is recycled back into the extraction process and this output is replaced by fresh water from Beaver Creek Reservoir to maintain the surface elevation at 308.5 m above sea level. Over time, water from the surrounding mine closure landscape is expected to support the inflow of water to BML and outflow will be to the Athabasca River. Base Mine Lake contains approximately 32 Mm^3 of oil sands process-affected water and covers an area of approximately 7.7 km^2.

Figure 3-1: Satellite image of the Syncrude Mildred Lake mine (Image provided by Syncrude and Hatfield Consultants).

3.2 Field Sample Collection

Samples of FFT were collected from BML in August 2016, March 2017 and July 2017. During each sampling campaign, FFT was collected from platforms located in the southwest corner (P3), center (P1) and northeast corner (P2) of BML (Figure 3-2). Since the pit bottom elevation follows the final mine pit topography, FFT thickness is not uniform and settlement rates are spatially variable. Self-weight consolidation drives settlement (Dompierre et al., 2017) and areas with greater FFT thickness typically exhibit greater settlement rates. This process also controls dewatering and, therefore, pore-water expression to the cap also exhibits spatial

variability. Collecting samples at each of the three platforms helped ensure that the FFT settlement heterogeneity was captured.

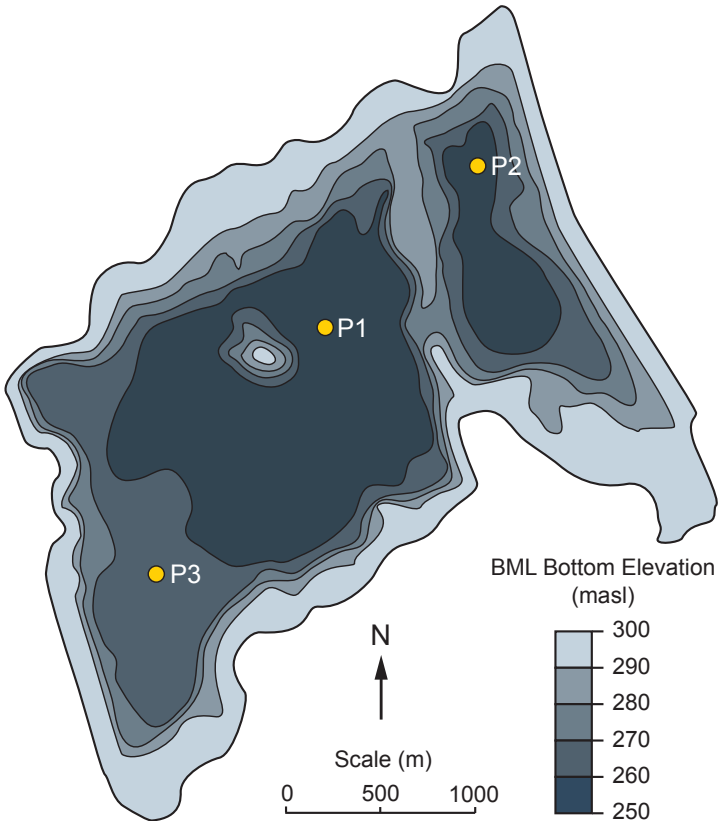

Figure 3-2: Base Mine Lake pit bottom elevation and platform locations (Dompierre et al., 2016). The water surface elevation is maintained at approximately 308.5 m above sea level.

3.2.1 Sampling Equipment

Samples were collected using two custom-built samplers deployed from an overhead winch system on a work boat with a moon pool in the deck. The fixed interval sampler (Dompierre et al., 2017) was used to collect samples across the TWI and the fluid sampler (Dompierre et al., 2016, Supplementary Content) was used to collect deeper samples with a higher solid content. The TWI depth was estimated in the field by sonar and later confirmed by measuring solid content.

The fixed interval sampler consisted of 20 discrete sampling cylinders positioned 10 cm apart from each other (Figure 3-3). Each cylinder had a volume of 250 mL and contained an internal piston that was attached to a compressed gas source. Compressed nitrogen gas (275 kPa) was used to keep the pistons closed as the sampler was slowly lowered into the lake. The sampler

was positioned with approximately four cylinders above the TWI, one at the interface and fifteen below the interface. This positioning resulted in 20 samples ranging from approximately 0.4 m above the TWI to approximately 1.5 m below the interface. After a 10-minute settlement period, the pistons were slowly retracted. The sampler was returned to the surface after approximately 10 minutes and FFT from each piston was extruded into a 250 mL high density polyethylene (HDPE) bottle.

The fluid sampler consisted of a single 4 L sampling cylinder with an internal piston and an upper weight to keep the sampler in an upright position (Figure 3-3). Compressed gas was used to keep the sampler closed as it was lowered to the desired sample depth. After a 10-minute settlement period the piston was pulled back to the open position and after approximately 15 minutes the fluid sampler was brought to the surface. The fine tailings were extruded directly from the fluid sampler into 250 mL HDPE bottles.

Figure 3-3: Fixed interval sampler (left) and fluid sampler (right).

3.2.2 Sample Collection Depths

The depths at which samples were collected varied during each sampling campaign (Table 3-1). For all three campaigns, the fixed interval sampler was used to collect samples across the TWI to ensure sufficient spatial resolution to capture sharp physicochemical gradients. In August 2016, analysis of FFT biogeochemistry within the first 10 m below the TWI was conducted. March 2017 involved a smaller sampling campaign to identify potential seasonal changes in FFT biogeochemistry within the first 1.5 m below the TWI. In July 2017, a larger sampling campaign was conducted to retrieve samples throughout the FFT deposit. The fluid sampler was lowered until it encountered resistance from the higher proportion of coarse sand near the pit bottom.

Table 3-1: Minimum and maximum sampling depths at the three platforms for each sampling campaign. Depth values are stated as meters below the TWI.

Location	Campaign	Sampling Depth (m)	
		Minimum	Maximum
Platform 1	August 2016	−0.35	10.55
	March 2017	−0.35	1.55
	July 2017	−0.40	40.00
Platform 2	August 2016	−0.55	9.85
	March 2017	−0.45	1.45
	July 2017	−0.75	17.75
Platform 3	August 2016	−0.40	9.70
	March 2017	−0.55	1.35
	July 2017	−0.45	33.35

3.2.3 Sample Collection for Geochemical and Microbiological Analysis

The bulk 250 mL FFT samples collected directly from the samplers were used for geochemical analysis. The number of samples collected at each platform varied between each sampling campaign (Table 3-2). All samples were stored in coolers with ice packs for 2 to 10 hours until they could be transported to the Reclamation and Closure Research laboratory on the Mildred Lake site for analysis.

Subsamples for microbiological analysis were taken from the bulk 250 mL FFT samples. In 2016, subsamples were collected at the lab after bulk samples were centrifuged to separate the pore water and solids. A retractable blade sterilized with 70% (v/v) ethanol was used to cut the HDPE bottle and a sterile metal scoopula was used to transfer the solids to a sterile 50 mL conical polypropylene tube. Samples were then immediately stored at -20°C until further analysis. In 2017, subsamples were collected on the field boat immediately after sample collection. Approximately 40 mL of FFT was poured from the bulk sample into a sterile 50 mL conical polypropylene tube. Subsamples were stored in a cooler with ice packs for 2 to 10 hours until transportation to the lab on site. At the lab, the subsamples were centrifuged at 3 300 x g for 40 minutes and the supernatant was poured off and discarded. The remaining solids were stored at -20°C until further analysis. The depths at which subsamples were collected for microbiological analysis were determined based on previous knowledge of FFT geochemistry. Subsamples were taken at depths where past studies suggested Fe(III) reduction, SO_4 reduction and methanogenesis may be occurring (Table 3-2).

Table 3-2: Number of samples collected from each platform for geochemical and microbiological analysis.

Location	Campaign	Geochemistry	Microbiology
Platform 1	August 2016	45	9
	March 2017	20	4
	July 2017	40	7
Platform 2	August 2016	45	8
	March 2017	20	4
	July 2017	36	7
Platform 3	August 2016	45	9
	March 2017	20	4
	July 2017	39	7

3.3 Geochemistry Methods

3.3.1 pH, Eh and Temperature

Temperature and pH were measured on the boat immediately following sample collection in both summer campaigns. The pH electrode (Thermo Scientific, model 8172BNWP) was calibrated using a 3-point calibration with NIST-traceable pH 4, 7 and 10 buffer solutions (Thermo Scientific). Reduction-oxidation potential (Eh) was taken after samples had been transported to the lab due to time constraints for probe equilibration. The Eh electrode (Thermo Scientific, model 9678BNWP) accuracy was referenced against Light's (Light, 1972) and Zobell's (Nordstrom, 1977) standard solutions before measurements. The Eh measurements were taken only on July 2017 samples and a small portion of the August 2016 samples due to measurement drift and poor equilibration in previous sampling campaigns. Measured Eh values were corrected to the standard hydrogen electrode.

3.3.2 Pore-Water Extraction and Analysis

After transportation to the lab, samples were refrigerated (i.e., +4°C in the dark) for up to 12 hours before processing. Pore water was extracted from the 250 mL samples by centrifugation at 8 500 x g for 30 minutes. Approximately 50 to 225 mL of pore water was extracted per 250 mL HDPE bottle depending on the depth at which the sample was collected. Electrical conductivity (EC), alkalinity (as $CaCO_3$), sulfide (S^{2-}) and ammonia (NH_3-N) were measured immediately after centrifugation due to the time sensitivity associated with these analyses. Each analysis was measured on pore water that had been passed through a 0.45 µm polyesthersulfone (PES) syringe filter using 30 mL syringes (HSW GmbH, Germany). Collectively, these analyses required approximately 30 mL of water per sample. The conductivity probe (Thermo Scientific, model 013005MD) was calibrated using a 1413 µS/cm NaCl solution (Thermo Scientific) and corrected for temperature. Alkalinity was measured using a digital titrator to the bromocresol green – methyl red endpoint using 1.6 N sulfuric acid. Dissolved S^{2-} and NH_3-N were measured on a portable spectrophotometer (HACH Company, model DR2800) using the methylene blue method (HACH Method 8131) and salicylate method (HACH Method 10205), respectively. The results from the salicylate method are a sum of both inorganic NH_4^+ and NH_3, however NH_4^+ likely dominates the aqueous speciation at the measured pH values (Dompierre et al., 2016). These parameters were not measured during the March 2017 sampling campaign.

Remaining pore water was filtered and preserved for quantification of major anions, cations and trace elements. Approximately 15 to 30 mL of water was filtered for each of these analyses and all samples were refrigerated until analysis. Anions were quantified via ion chromatography and water filtered for this instrument was passed through a 0.45 μm PES filter and stored in a 30 mL HDPE narrow mouth bottle. The ion chromatography method detection limit was 0.05 mg L^{-1}. Major cations were quantified by inductively coupled plasma optical emission spectrometry. Water preserved for this instrument was passed through a 0.2 μm PES filter into an HDPE narrow mouth bottle and acidified to a pH less than 2 using trace metal grade nitric acid (Omnitrace, EMD Millipore, USA). The method detection limit for S was 0.026 mg L^{-1}. Trace element concentrations were determined by inductively coupled plasma mass spectrometry. Water designated for this instrument was preserved using the same method as cations in August 2016 and March 2017. The method was modified slightly in July 2017 and the water was passed through a 0.1 μm PES filter. The method detection limit for Fe and Mn were 0.62 μg L^{-1} and 0.056 μg L^{-1}, respectively.

3.4 Microbiology Methods

3.4.1 DNA Extraction and Quantification

Genomic deoxyribonucleic acid (DNA) was extracted from each sample in triplicate using the FastDNA SPIN Kit for Soil (MP Biomedicals, CA, USA). The FastPrep 120 instrument (Thermo Savant) was used to homogenize samples for 40 seconds at a speed setting of 6.0. The extraction protocol suggested by the manufacturer was modified at three stages to increase the quality and quantity of DNA yields. First, the cell disruption steps were repeated twice and the resulting product was pooled before adding the binding matrix solution. The ethanol wash step was repeated three times to ensure organics had been washed away. Finally, DNA was eluted twice with deoxyribonuclease-free water to obtain a final volume ranging from 100 to 150 μL.

The extracted DNA was quantified using a Qubit 2.0 Fluorometer (Invitrogen, Life Technologies, CA, USA) and a Qubit High Sensitivity dsDNA Assay Kit (Life Technologies, CA, USA). The quality of extracted DNA was measured using an Epoch Microplate Spectrophotometer with Take3 plate (BioTek, VT, USA). High quality DNA is characterized by an $A_{260/280}$ value

between 1.8 and 2.0 and an $A_{260/230}$ value greater than 2.0 (Mahmoudi et al., 2011). The extracted DNA was stored at -20°C until further analysis.

3.4.2 High-Throughput Amplicon Sequencing

High-throughput amplicon sequencing was conducted on aliquots of extracted DNA using the Illumina MiSeq platform (Illumina, CA, USA). The DNA was amplified and purified in preparation for sequencing at the University of Calgary using a modified Illumina protocol (Illumina, 2013). Specifically, the V4 region of the 16S rRNA gene in Bacteria and Archaea was amplified through polymerase chain reaction (PCR) using the primers 515FB (5'-GTGYCAGCMGCCGCGGTAA-3') and 806RB (5'-GGACTACNVGGGTWTCTAAT-3'). These primers are consistent with primers used for the Earth Microbiome Project (Walters et al., 2015). The product was run on a 1% agarose gel to ensure amplicon size was correct and no extraneous bands were present. The product was then purified using magnetic beads (Omega Bio-Tek, GA, USA). A second PCR reaction was then conducted to attach dual-index barcodes and adapter sequences to the amplicons. This PCR product was also run on a 1% agarose gel and bead-purified. A no template control was included in both PCR reactions and it did not amplify. The final amplicon samples were quantified using a Qubit Fluorometer (Invitrogen, Life Technologies, CA, USA) and normalized quantities of amplicons were prepared for each sample by diluting to 4 nM DNA. Aliquots of 5 µL from 176 samples were pooled into a single tube and stored at -20°C until sequencing. Samples were sequenced on a MiSeq machine (Alberta Children's Hospital, University of Calgary) in December 2017 using a v3 chemistry (600-cycle) reagent kit (Illumina, CA, USA).

3.4.3 Bioinformatics Processing

The high-throughput amplicon sequencing data was processed using the mothur bioinformatics software package and MiSeq standard operating procedure (Kozich et al., 2013; Schloss et al., 2009). Briefly, contigs were formed from the paired MiSeq sequencing reads and sequences were removed if they contained any ambiguous base pairs, were shorter than 200 base pairs or longer than 375 base pairs. Sequences were then aligned against the V4 region of the Silva 16S rRNA gene database and any overhanging sequences were removed. Chimeras were identified and removed using the VSEARCH algorithm (Rognes et al., 2016). Taxonomy was assigned to sequences with an 80% confidence sequence classification cutoff against the Silva 132 database.

It should be noted that the Silva 132 release rearranged the *Proteobacteria* phylum and organized *Epsilonproteobacteria* as its own phylum and *Betaproteobacteria* as an order within the *Gammaproteobacteria* class (Parks et al., 2018). Finally, sequences belonging to Eukaryota, chloroplasts, mitochondria and unknown were removed (0.4% of the total sequence reads). These sequences were removed because the primers chosen were designed to only amplify prokaryotes. The read numbers for each set of triplicates were then compared at the phylum and genus level to investigate reproducibility and the numbers among triplicate samples were similar. The triplicates were then merged to improve data visualization and the sequences were subsampled to the lowest read number, which was 34 200 reads. Subsampling the total sequences in each sample ensured the samples were normalized for diversity comparisons.

Sequences were clustered at 97% sequence similarity into operational taxonomic units (OTUs) and classified using the Silva 132 database. Alpha diversity was examined by calculating Good's coverage, Inverse Simpson Index and species observed in each sample. Good's coverage estimated what percent of the total species were observed in a sample, the Inverse Simpson Index measured diversity and the species observed measured richness. Distance matrices were created using theta Yue-Clayton and Jaccard calculations to examine beta diversity (Yue and Clayton, 2005). Theta Yue-Clayton calculations were used for comparison of microbial community structure (presence and relative abundance of OTUs). Jaccard calculations were used for comparison of community membership (presence of OTUs). The theta Yue-Clayton calculations therefore incorporated the proportion of shared and not shared OTUs, whereas the Jaccard calculations compared only the shared OTUs between samples. Beta diversity was illustrated through the creation of dendrograms and non-metric multidimensional scaling (NMDS) plots based on the Jaccard and theta Yue-Clayton distance matrices. Dendrograms were generated to examine the similarity of samples to one another. The NMDS ordination plotting provided a sample community composition comparison and similar samples were plotted closer to one another than dissimilar samples. The correlation of the relative abundance of each OTU with the two axes in the NMDS data was calculated with the Spearman correlation method. Select contributors responsible for shifting the samples along the two axes were plotted over the respective NMDS plot as a biplot.

CHAPTER 4: RESULTS

4.1 Geochemistry

4.1.1 Geochemical Setting

The TWI depth was verified at each location through measurement of the solids weight percent. Values increased to over 30% (w/w) across the TWI. The solids content gradually increased with depth and generally reached values over 50% (w/w) near the pit bottom. The TWI increased in depth relative to the water surface at all platforms during the two-year sampling period (Table 4-1).

Table 4-1: Depth of the TWI relative to the water cap surface during each sampling campaign. The water surface elevation was maintained at approximately 308.5 m above sea level.

Location	TWI Depth (m)		
	August 2016	**March 2017**	**July 2017**
Platform 1	9.45	9.60	10.00
Platform 2	11.15	9.70	11.65
Platform 3	9.30	8.80	9.55

The median temperature in the water cap samples was 18 °C and values ranged from 16.6 to 21.1 °C. Temperatures decreased below the TWI and the median temperature in the FFT deposit was 14.5 °C. Temperatures varied with depth in the FFT and maximum temperatures were observed at depths between 10 and 20 m below the TWI.

The pH values in the water cap ranged from 8.0 to 8.4 and decreased sharply across the TWI to below 7.8 (Figure 4-1). Overall, pH values gradually decreased with depth in the FFT deposit. The pH values remained generally consistent over time and depth trends varied slightly among platforms. In both summer campaigns, a noticeable increase in pH was observed within the first 2 m below the TWI at Platform 3. This increase also occurred at Platform 1 during the March

2017 sampling campaign. The pH peaked at approximately 1.5 m below the interface and values were generally above 8.0 (Figure 4-1). Below this peak, pH values at Platform 3 subsequently decreased to approximately 7.1 at 2.5 m below the interface. The pH values were consistent at depths greater than 15 m below the TWI and generally remained between 6.9 and 7.3.

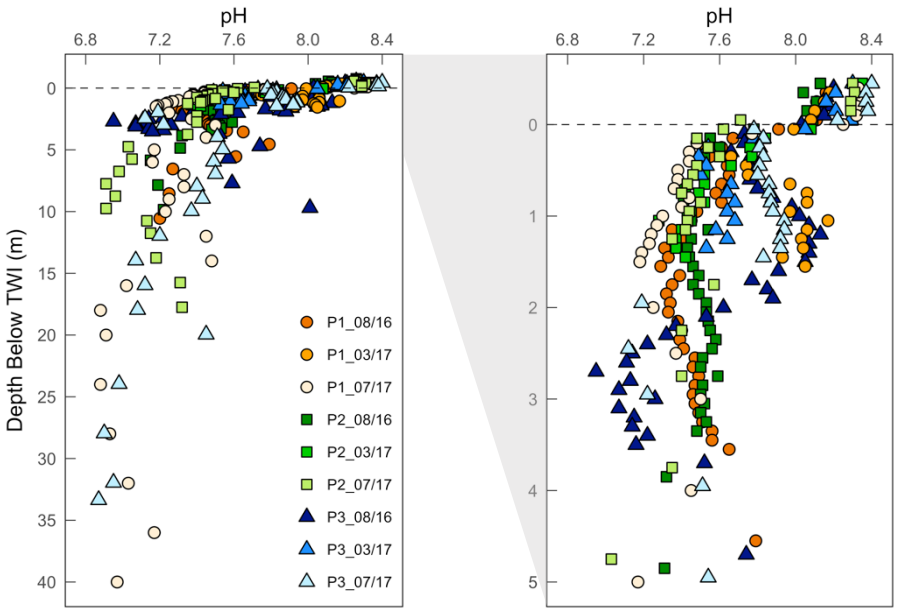

Figure 4-1: pH depth profile for all samples, extending to 40 m (left) and 5 m (right) below the TWI.

Alkalinity in the water cap ranged from 570 to 815 mg L^{-1} and increased to over 1000 mg L^{-1} below the TWI (Figure 4-2). Slight increases with depth were observed in the FFT and values over 1350 mg L^{-1} were observed more than 15 m below the TWI. Alkalinity profiles were generally consistent among platforms and exhibited limited temporal variability.

Electrical conductivity ranged from 2.60 to 2.96 mS cm^{-1} in the water cap (Figure 4-2), but increased sharply across the TWI reaching a maximum value of 5.3 mS cm^{-1} within the FFT. The EC trends remained consistent at all locations throughout the first 5 m below the TWI. Platforms 1 and 3 exhibited similar peaks with depth, the EC at Platform 2 remained at approximately 4.20 mS cm^{-1} with depth. Conductivity values were consistent between sampling campaigns.

The Cl concentrations followed similar trends to EC (Figure 4-2). Dissolved Cl increased below the TWI and the median concentration in the FFT was 552 mg L^{-1}. Maximum concentrations were observed at depths between 10 and 20 m below the TWI.

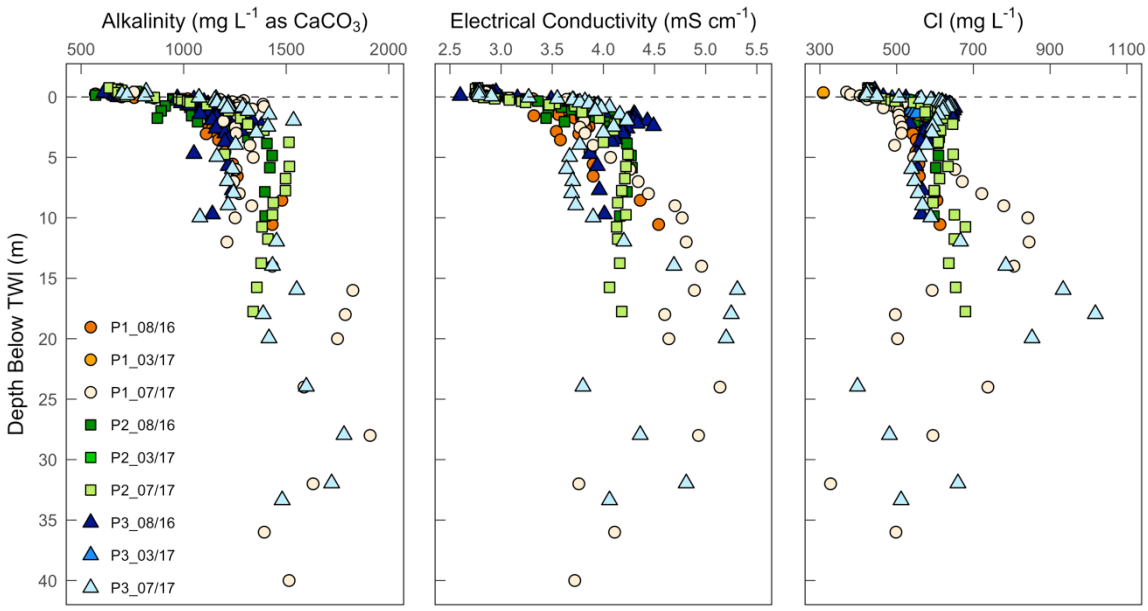

Figure 4-2: Alkalinity (left), electrical conductivity (center) and Cl (right) depth profiles for August 2016 and July 2017.

The Eh values were not representative of the anoxic conditions in the FFT deposit. After correcting the measured Eh values to the standard hydrogen electrode, redox potentials in the water cap ranged from +300 to +420 mV. Values decreased in the FFT deposit, however, they remained mostly positive and did not exhibit any distinct depth-dependent trends. The negative values ranged from 0 to -63 mV and were mostly isolated to a 1 m zone immediately below the TWI. Discrepancy between measured and theoretical Eh values can arise due to the absence of electroactive species (Markelova, 2017). The presence of species produced in strongly reducing conditions, specifically $\sum H_2S$ and CH_4, were indicative of anoxic conditions in the FFT deposit.

4.1.2 Nitrogen Species

Pore-water NO_3 concentrations were commonly below the detection limit in both the water cap and FFT pore water. Low concentrations were detected in the water cap of the March 2017 samples with values ranging from 0.44 to 1.01 mg L^{-1}. Dissolved NO_3 was also detected at Platform 1 in July 2017 at scattered depths with concentrations ranging from 0.1 to 0.5 mg L^{-1}. Additionally, pore-water NO_2 concentrations were below the detection limit in all FFT samples. Dissolved NO_2 was detected only in the water cap of the March 2017 samples with concentrations ranging from 0.23 to 0.28 mg L^{-1}.

Total NH_3-N concentrations were typically below 1.0 mg L^{-1} in the water cap and increased below the TWI at all platforms (Figure 4-3). Pore-water NH_3-N concentrations at Platform 1 increased steadily below the interface and exhibited a distinct peak at approximately 4.5 m below the TWI. Concentrations below this peak were slightly variable between 2016 and 2017. Similarly, the NH_3-N concentrations at Platform 3 increased gradually below the TWI. A peak was exhibited at 8.0 m below the TWI and concentrations were approximately 22 mg L^{-1}. The concentrations at Platform 3 were consistent between 2016 and 2017. The concentrations at Platforms 1 and 3 averaged 11 ± 4.3 mg L^{-1} (n=27) at depths below these peaks in the FFT deposit. The NH_3-N concentrations at Platform 2 also increased below the TWI, however a distinct peak was not observed. The concentrations increased for approximately 2.5 m below the TWI and then subsequently remained at an average concentration of 13 ± 5.1 mg L^{-1} (n=22) throughout the FFT deposit. The NH_3-N concentrations at Platform 2 were also consistent between 2016 and 2017.

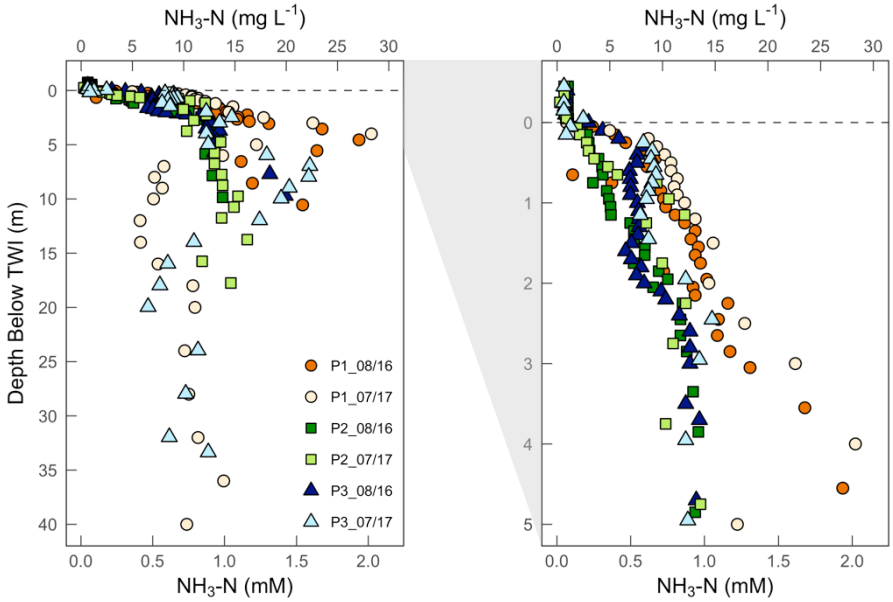

Figure 4-3: Depth profile of NH_3-N for August 2016 and July 2017 samples extending 40 m (left) and 5 m (right) below the TWI.

4.1.3 Iron and Manganese

Total dissolved Fe concentrations were low throughout the FFT deposit (Figure 4-4). Concentrations in the water cap ranged from 0.001 to 0.57 mg L^{-1} and values did not distinctly increase or decrease directly below the TWI. Dissolved Fe concentrations remained consistent

within the upper 10 m below the TWI and values were higher in the August 2016 samples. Average dissolved Fe concentrations in the FFT deposit for August 2016 were 0.23 ± 0.07 mg L^{-1} (*n*=77). Average concentrations for the upper 10 m in July 2017 were 0.06 ± 0.06 mg L^{-1} (*n*=66). A gradual increase in dissolved Fe concentrations was observed at all platforms at depths greater than 10 m below the interface. Concentrations at Platforms 1, 2 and 3 increased to values of 0.50, 0.31 and 0.88 mg L^{-1}, respectively. The reported values represent total dissolved Fe concentrations. It is likely that the dissolved Fe pool is comprised of Fe(II) because Fe(III) is insoluble at circumneutral pH values and Fe(II) is soluble under anoxic conditions at the measured pH (Dompierre et al., 2016).

Total dissolved Mn concentrations were also low throughout the FFT deposit (Figure 4-4). Dissolved Mn concentrations in the water cap ranged from 0.040 to 0.12 mg L^{-1} and values did not distinctly increase or decrease directly below the TWI. Concentrations varied slightly among locations and concentrations in the FFT deposit ranged from 0.007 to 0.16 mg L^{-1}. Maximum dissolved Mn concentrations for each platform occurred at different depths in the FFT deposit, ranging from 9 to 28 m below the TWI.

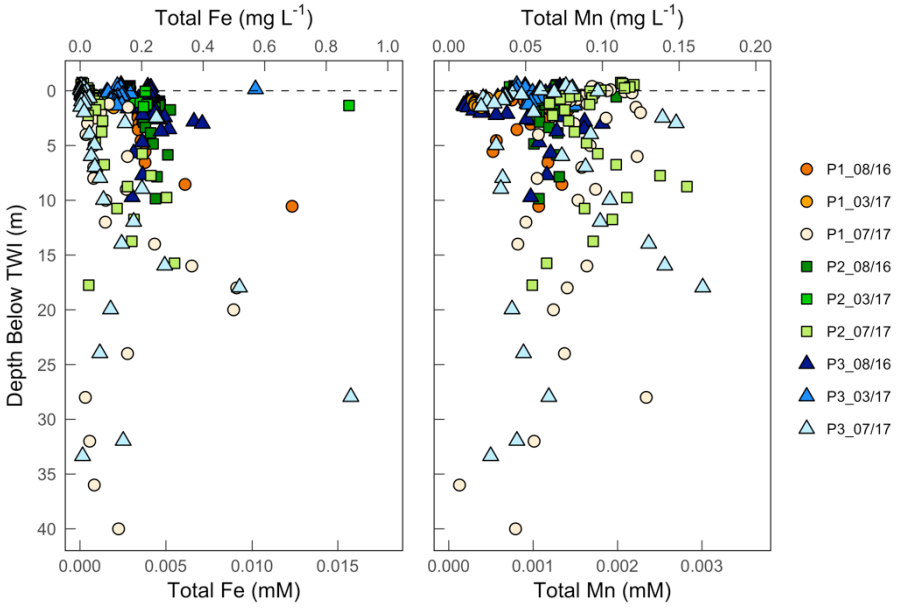

Figure 4-4: Depth profile of total dissolved Fe (left) and Mn (right) for all sampling points.

4.1.4 Sulfur Species

The median SO_4 value in the water cap was 177 mg L^{-1} and concentrations decreased sharply to less than 50 mg L^{-1} across the TWI (Figure 4-5). The median SO_4 value in the FFT deposit was 13 mg L^{-1} and concentrations typically remained low (less than 5 mg L^{-1}) at depths greater than 5 m below the TWI. The depth trends were consistent between 2016 and 2017, as well as among the locations.

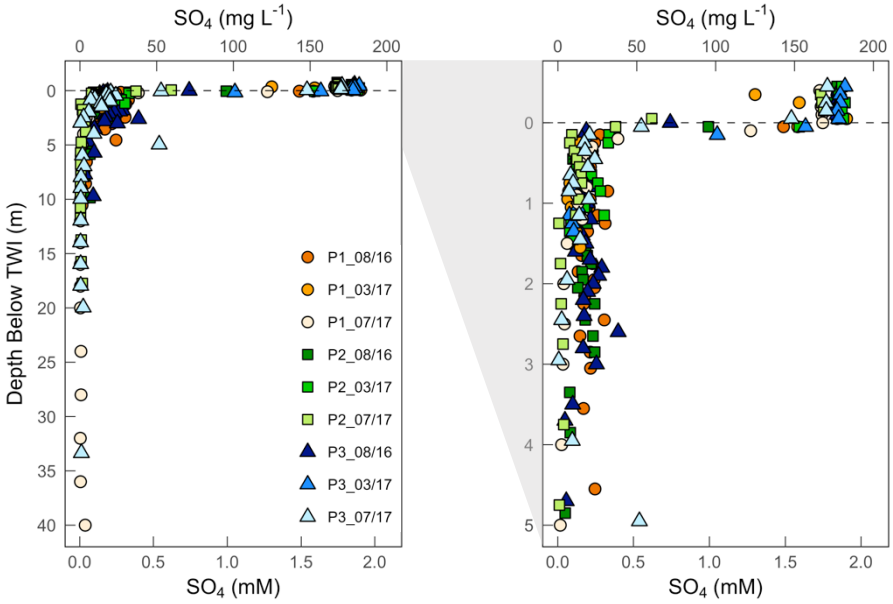

Figure 4-5: SO_4 depth profile for all samples, extending to 40 m (left) and 5 m (right) below the TWI.

The $\sum H_2S$ concentrations in the water cap were consistently below 35 µg L^{-1} and increased across the TWI at all platforms (Figure 4-6). A zone of elevated $\sum H_2S$ concentrations (up to 700 µg L^{-1}) occurred within the upper 0.5 m of the FFT deposit and maximum values were observed within the upper 5 m. Considerable $\sum H_2S$ concentrations over 1000 µg L^{-1} were measured at Platform 3 during both sampling campaigns and at Platform 1 in July 2017. The $\sum H_2S$ concentrations at Platform 2 were relatively low compared to the other platforms and a distinct peak in concentrations was not observed. Pore-water $\sum H_2S$ concentrations were low (less than 100 µg L^{-1}) at all platforms at depths greater than 15 m below the TWI.

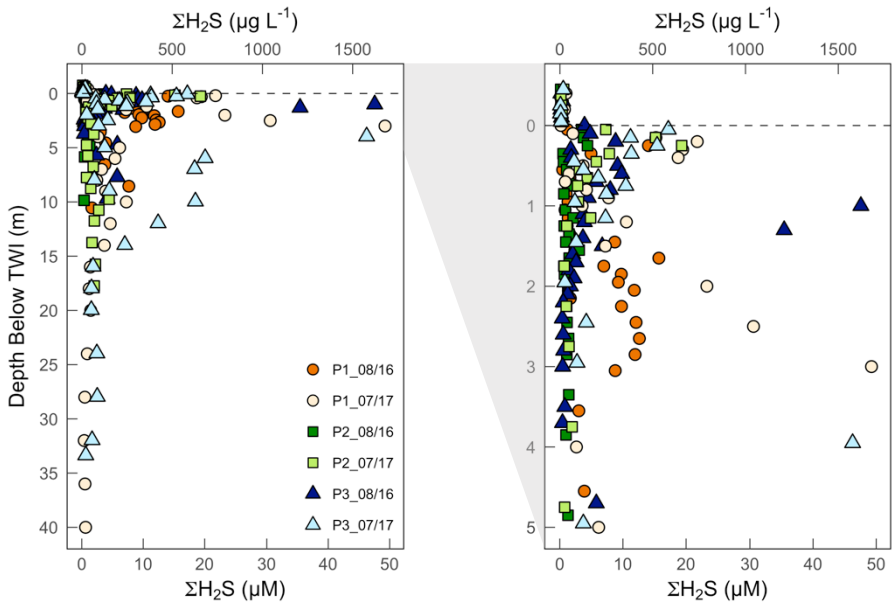

Figure 4-6: $\sum H_2S$ depth profile for August 2016 and July 2017 samples, extending to 40 m (left) and 5 m (right) below the TWI.

Although measurements for specific SOIs was not conducted, the proportion of SOIs in the total S pool was calculated by assuming the concentration of total S was equal to the sum of the concentration of SO_4, $\sum H_2S$ species and SOI species (Equation 4.1). Total S concentrations were highest in the water cap, ranging from 1.8 to 2.2 mmol L^{-1}, and SO_4 comprised much of the total S pool (Figure 4-7). Total S concentrations decreased in the FFT deposit to values predominantly below 0.5 mmol L^{-1}, due to the sharp decrease in SO_4 concentrations below the interface. The total S pool was dominated by SOI species in FFT and this trend was recognized in both the August 2016 and July 2017 samples.

$$[S_T] = [SO_4^{2-}] + [\sum H_2S] + [\sum SOI] \quad (4.1)$$

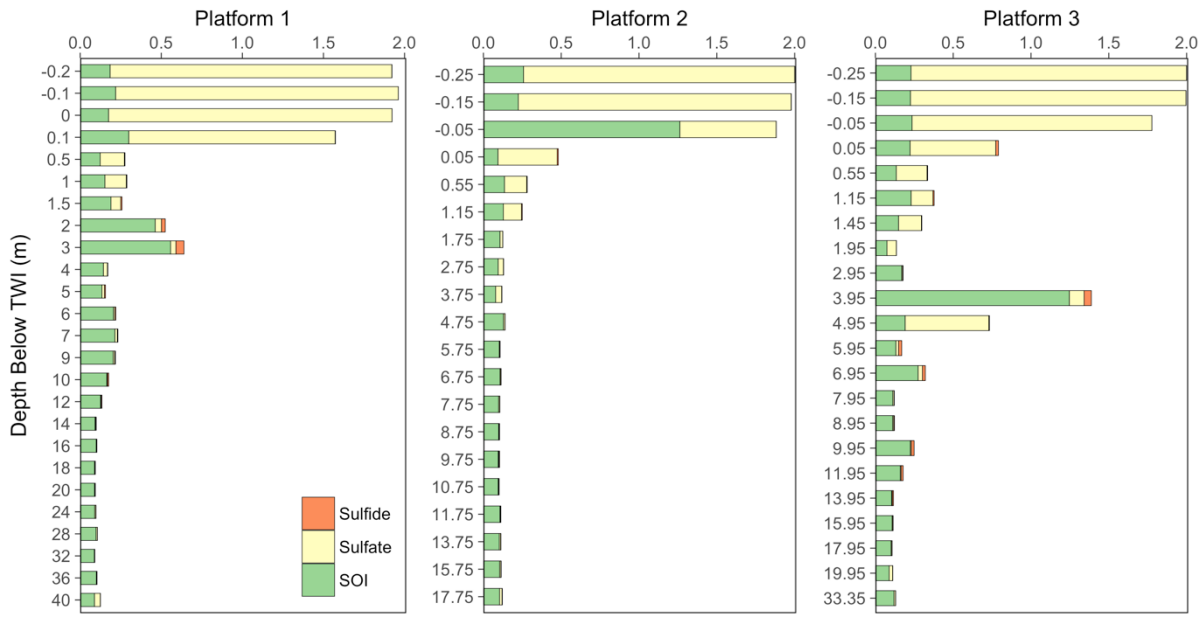

Figure 4-7: Stacked bar plot representing the concentrations of S species in the total S pool for July 2017. All values are in mmol L^{-1}.

4.1.5 Methane

Dissolved CH_4 concentrations in the water cap were generally less than 2 mg L^{-1} at each platform (Figure 4-8). The $CH_{4(aq)}$ concentrations gradually increased within the first 1.5 m below the TWI and remained elevated throughout the depth profile. At Platforms 1 and 2, concentrations increased to approximately 40 mg L^{-1} by 1 m below the interface and the values were consistent between 2016 and 2017. Below this initial increase, the average concentration was 47 ± 10 mg L^{-1} (n=15) at Platform 1 and 59 ± 10 mg L^{-1} (n=13) at Platform 2. The $CH_{4(aq)}$ concentrations slightly increased with depth at Platform 3 and similar depth trends were observed between years. The average concentration in the FFT deposit at Platform 3 was 37 ± 13 mg L^{-1} (n=37).

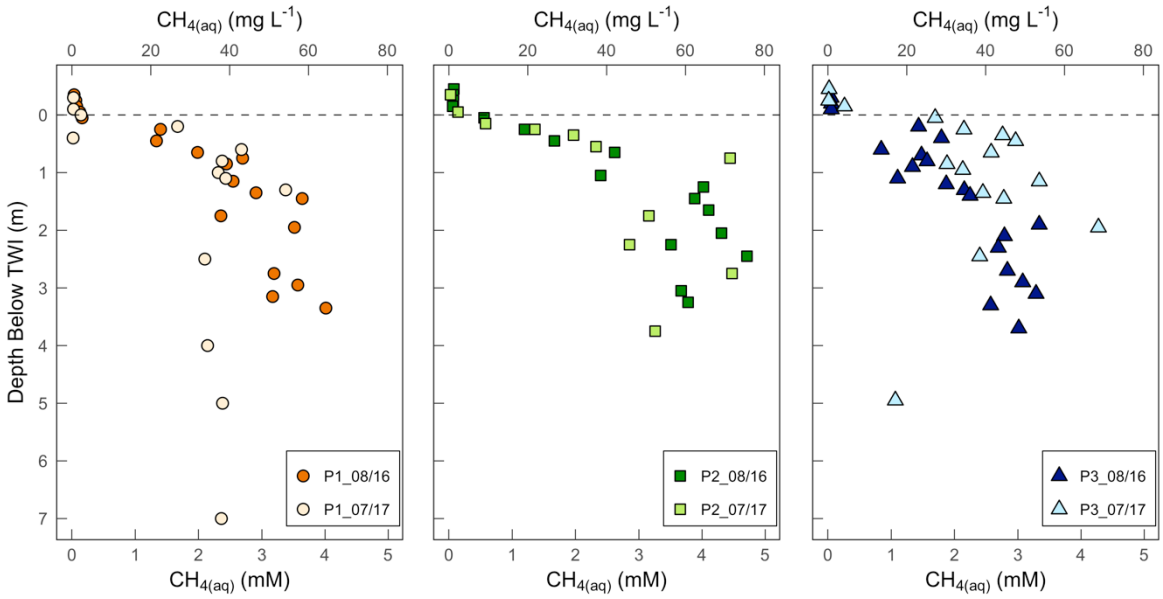

Figure 4-8: Dissolved CH_4 concentrations for Platform 1 (left), Platform 2 (center) and Platform 3 (right) in August 2016 and July 2017.

4.2 Microbiology

4.2.1 Alpha and Beta Diversity

Diversity was highest at the TWI and generally decreased with depth (Figure 4-9). The depth-dependent diversity trends differed slightly among the three platforms, however the calculated values were consistent over time. Diversity values calculated using the Shannon Index (Table B-2) demonstrated similar trends. The number of species observed, or the number of OTUs observed, also decreased with depth (Figure 4-10). The number of species observed sharply decreased within the upper 2 m of the FFT deposit at each platform and the values were consistent over time. Estimates of species richness calculated with the Chao Estimator and Ace Estimator (Table B-2) further demonstrated that the greatest richness occurred at the TWI. The Good's coverage for all samples was above 97% (Table B-2), indicating a high sample coverage for the sequencing results.

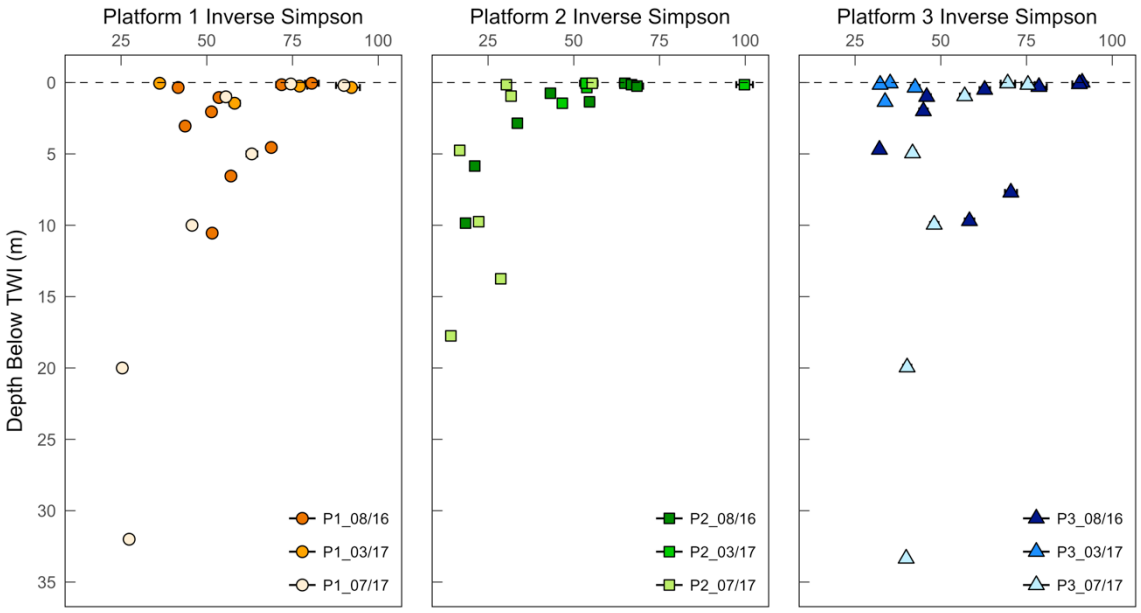

Figure 4-9: Inverse Simpson Index values for each sample point. Greater values represent a greater diversity. The error bars represent the high and low confidence intervals. Some error bars fell within the range of the symbol and were obscured. Each sample was subsampled to 34 200 reads for this calculation.

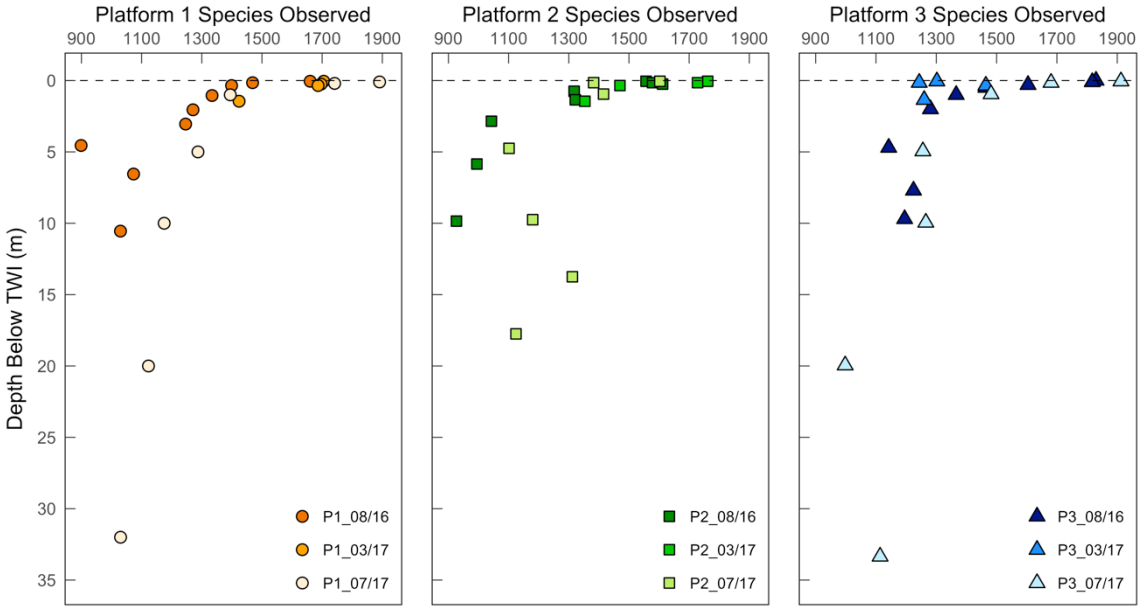

Figure 4-10: Number of species observed in each sample. Each sample was subsampled to 34 200 reads for this analysis.

The dendrogram created using theta Yue-Clayton calculations did not show specific clustering among samples based on location, sampling time or depth (Figure B-1). The dendrogram created using Jaccard calculations clustered samples that ranged from 0 to 2 m below the TWI and samples deeper than 2 m below the interface (Figure B-2). The NMDS plot created using Jaccard calculations had an R^2 value of 0.59 and was not further analyzed due to this low value. The NMDS plot created using theta Yue-Clayton calculations had an R^2 value of 0.88. Spearman's correlation calculations identified *Methanoregula, Methanosaeta, Peptococcaceae* SCADC (short-chain alkane-degrading culture) and unclassified *Desulfobacteraceae* as select OTUs responsible for shifting the samples along the two axes of the plot (Figure 4-11). The vector length of these OTUs were 0.950, 0.954, 0.963 and 0.892, respectively.

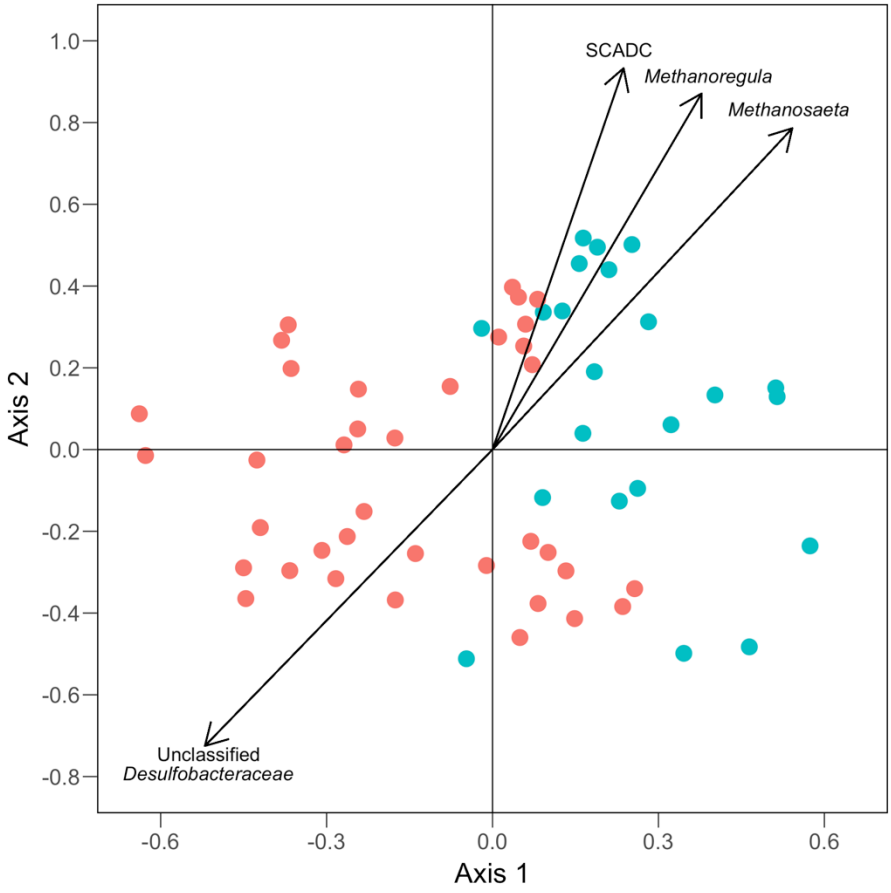

Figure 4-11: Two-dimensional NMDS plot created with theta Yue-Clayton distance matrix. The red dots are representative of samples ranging from 0 to 2 m below the TWI and the blue dots represent samples deeper than 2 m below the interface. The vectors represent select OTUs that influence the position of the samples along the two axes.

4.2.2 Overall Microbial Community Structure

The FFT microbial community was dominated by Bacteria and the read percentages classified to this domain were highest at the TWI (up to 99%). Sequencing reads classified to archaeal taxa were low near the TWI (1 to 2%) and increased with depth (10 to 19%). The most abundant phyla in the FFT deposit were *Proteobacteria,* followed by *Chloroflexi, Firmicutes, Actinobacteria, Euryarchaeota, Bacteroidetes* and *Tenericutes*. Unclassified Bacteria were also present in all FFT samples in low sequence abundance (1 to 5%). Similar trends and number of sequencing reads were observed among sampling campaigns. The July 2017 data was chosen to depict these trends (Figure 4-12) because it included samples from the entire depth profile.

The most abundant proteobacterial classes were the *Deltaproteobacteria*, followed by *Gammaproteobacteria* and *Alphaproteobacteria.* The proportion of deltaproteobacterial sequences were consistent with depth (Figure 4-12). The average percent abundance was 17 ± 3% (n=3) at the TWI and 14 ± 2% (n=3) near the pit bottom in July 2017. This class included putative SRB classified to the *Desulfobulbaceae* and *Desulfobacteraceae* families. Microbes classified to the *Syntrophaceae* family were also identified (2 to 6% of reads) and included the genera *Smithella* and *Syntrophus*. Sequences classified to taxa associated with Fe reduction were identified in the *Geobacteraceae* family. The proportion of these genera, *Geobacter* and *Geothermobacter*, did not exhibit distinct depth trends and each genus comprised up to 3% of the total sequencing reads.

The gammaproteobacterial sequence reads were most abundant at the TWI (Figure 4-12). The abundant families classified to this class were *Methylococcaceae* and *Methylomonaceae*, which include taxa capable of aerobic methanotrophy. The alphaproteobacterial sequence read abundance decreased slightly with depth (Figure 4-12) and the genus classified to the *Sphingomonadaceae* family with the greatest sequence read abundance was *Porphyrobacter.*

Sequence abundance corresponding to the *Betaproteobacteriales* order generally decreased with depth (Figure 4-12). This order contained microbes related to taxa capable of N cycling that were detected throughout the FFT deposit in low abundances. *Nitrosomonas*, an aerobic nitrifier, was detected at the TWI (up to 1% of reads) and *Thauera*, an anaerobic denitrifier, comprised up to 1% of the sequencing reads in the FFT. The most abundant genus classified to the *Burkholderiaceae* family was *Rhodoferax*, which contains iron-reducing bacteria. It comprised 2 to 13% of the sequencing reads at the TWI and was identified in the greatest proportions in the

March 2017 samples. Sequences classified to *Rhodoferax* were present throughout the FFT deposit, but decreased (to less than 2%) at depths greater than 10 m below the TWI. The genus *Hydrogenophaga* was also classified within the *Burkholderiaceae* family and comprised less than 1% of the sequencing reads throughout the FFT.

The proportion of sequencing reads classified to the *Chloroflexi* phylum greatly increased with depth. These reads were mostly classified to the *Anaerolineaceae* family, which contains taxa capable of fermentation. In July 2017, the *Anaerolineaceae* family comprised 7 to 9% of the sequence reads at the TWI and 21 to 30% of the reads near the pit bottom (Figure 4-12). Similar trends and proportions were observed in the August 2016 and March 2017 samples. The most abundant genera in the *Anaerolineaceae* family was uncultured and it was separated into multiple abundant OTUs. The proportion of sequencing reads classified to the *Firmicutes* phylum also increased with depth. The *Peptococcaceae* family comprised 1 to 6% of the sequencing reads at the TWI and 9 to 28% near the pit bottom in July 2017 (Figure 4-12). The greatest proportion of *Peptococcaceae* occurred at Platform 2 in both 2016 and 2017. The most abundant OTU in the *Peptococcaceae* family was classified as a short-chain alkane degrading culture (Tan et al., 2014).

The sequencing reads classified to the *Actinobacteria* phylum increased slightly with depth and contained sequences that classified as the order OPB41 (Figure 4-12). The abundant families within the *Bacteroidetes* phylum were *Flavobacteriaceae* and *vadin*HA17. The sequence reads corresponding to these families generally decreased with depth across all platforms (Figure 4-12). Sequences classified to the *Izimaplasmataceae* family within the *Tenericutes* phylum decreased with depth (Figure 4-12) and the OTUs within this family were all unclassified.

The most abundant families classified to the *Euryarchaeota* phylum were *Methanoregulaceae* and *Methanosaetaceae* and the proportion of these families increased with depth (Figure 4-12). The proportion of sequences classified to the *Methanoregulaceae* family increased from approximately 1% at the TWI to a maximum of 11% at Platform 1. The abundant genera classified to this family were *Methanoregula* and *Methanolinea*. These genera are associated with hydrogenotrophic methanogenesis. Sequencing reads classified to the *Methanosaetaceae* family comprised less than 1% of the total reads at the TWI and increased to approximately 6% in deeper FFT samples. The genera classified to the *Methanosaetaceae* family mainly consisted of *Methanosaeta* and this genus is associated with acetoclastic methanogenesis.

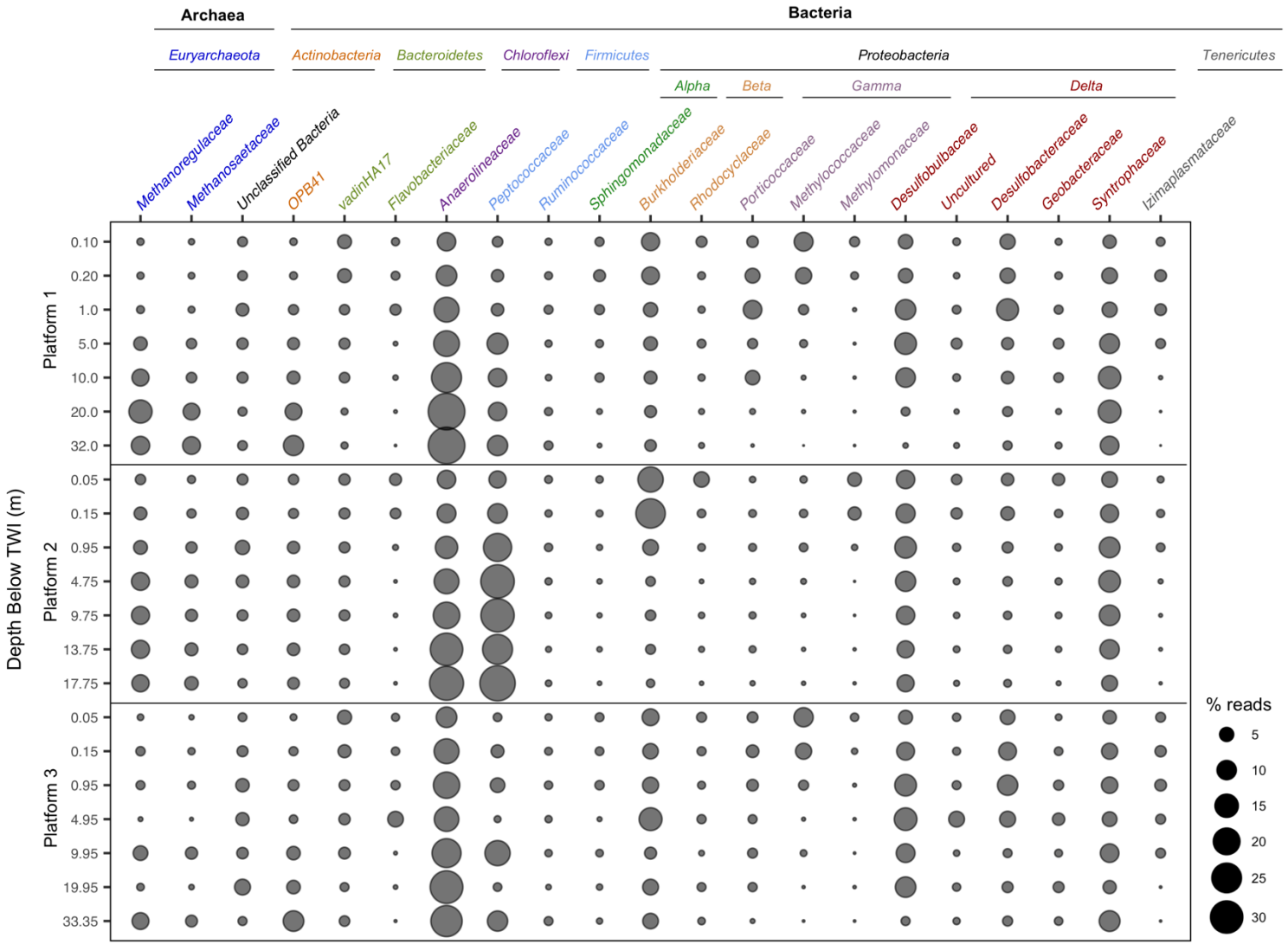

Figure 4-12: Bubble chart representing the 21 most abundant families in the July 2017 samples. Each bubble represents the percent of total sequencing reads for each sample. Each sample was subsampled to 34 200 reads.

4.2.3 Taxa Associated with Sulfur Cycling

Sequences classified to microbes associated with SO_4 reduction and SOI reduction/disproportionation were identified throughout the FFT deposit and comprised 3 to 29% of the total sequencing reads. The proportion of these sequences varied with depth and the lowest proportions were observed at depths greater than 20 m below the TWI (Figure 4-13). The abundant SRB-associated taxa were generally classified to the deltaproteobacterial families *Desulfobulbaceae* and *Desulfobacteraceae*. Unclassified genera belonging to these families were identified in all samples and the proportion of these sequences varied throughout the FFT deposit, ranging from 0 to 10% of the total reads. The putative SO_4-reducing genus with the highest number of sequencing reads was *Desulfoprunum* (Figure 4-13). It consistently comprised the highest proportion of sequences classified to SRB-associated taxa at Platform 2. Sequences classified to this genus did not exhibit a distinct depth-dependent trend at Platforms 1 and 3. Sequences classified to the putative SO_4-reducing genera *Desulfatiglans*, *Desulfatirhabdium* and *Desulfatitalea* were also identified at all platforms in varying proportions. Sequences classified to *Desulfuromonas*, a microbe associated with elemental S reduction, comprised less than 1% of the reads throughout the FFT. Sequences associated with microbes that grow by S disproportionation were also identified in FFT and were classified to the genera *Desulfurivibrio* and *Desulfocapsa*. The proportion of *Desulfurivibrio* remained below 1% of the sequencing reads at Platform 2. The percentage increased with depth at Platforms 1 and 3, and a maximum percentage of 10% was observed at Platform 1 in August 2016. The sequencing reads classified to *Desulfocapsa* generally comprised less than 1% of the total reads.

Reads classified as microbes associated with $\sum H_2S$ and SOI oxidation were also identified in the FFT samples. These reads were classified to the order *Betaproteobacteriales* (*Sulfuritalea* and *Sulfuricella),* class *Gammaproteobacteria* (*Thiocapsa)* and phylum *Epsilonproteobacteria* (*Sulfurimonas*, *Sulfuricurvum* and *Sulfurovum*). The putative sulfur-oxidizing microbes with the highest number of sequencing reads were *Sulfuritalea* and *Sulfurimonas*. The proportion of these microbes was generally highest at the TWI. Sequences classified to these genera comprised 4 to 6% of reads at the interface in March 2017 and 1 to 4% of the sequencing reads in August 2016 and July 2017.

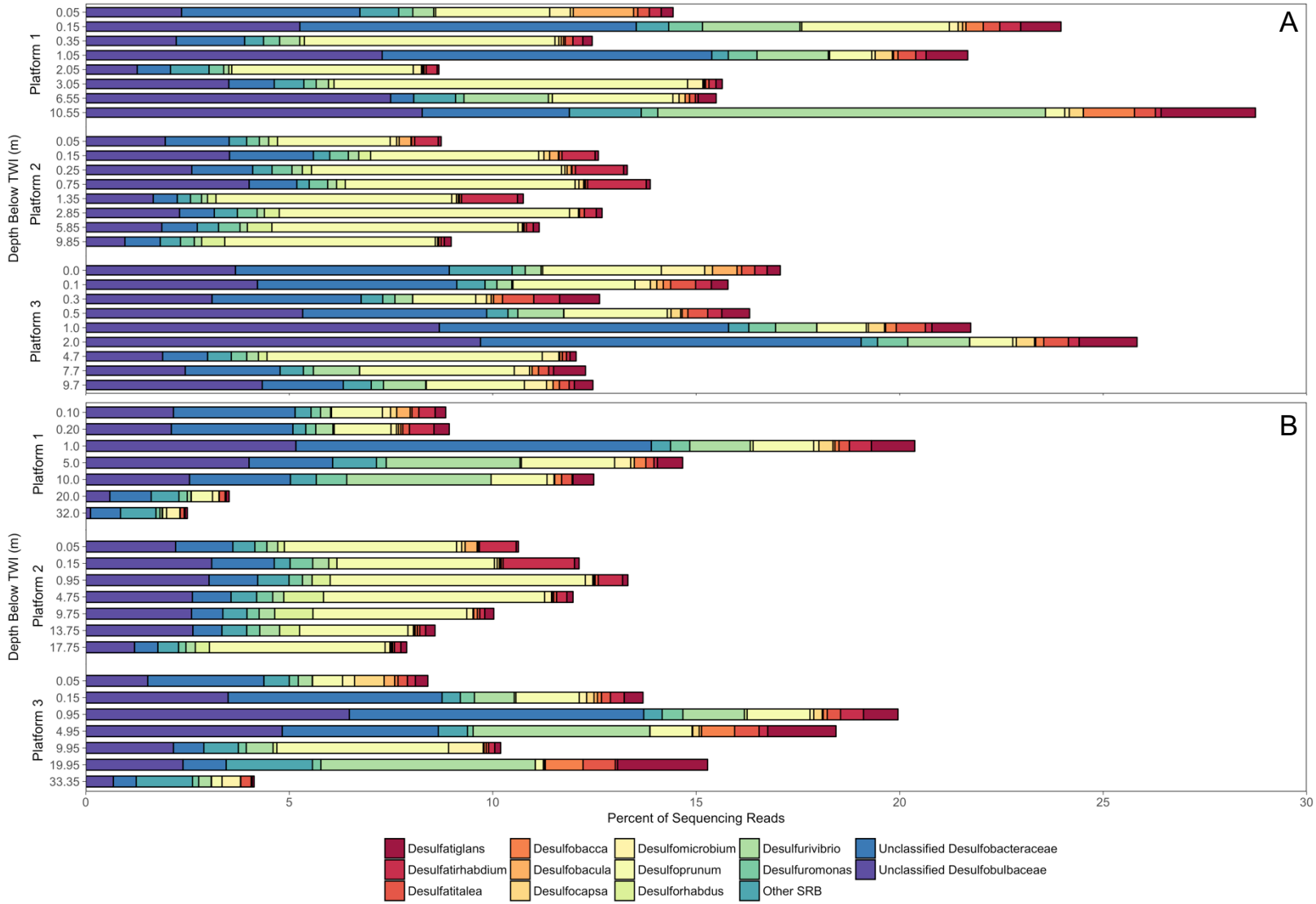

Figure 4-13: Stacked bar plot representing sequencing reads of potentially relevant sulfur reducers as a portion of the total reads in August 2016 (A) and July 2017 (B). Each sample was subsampled to 34 200 reads.

4.2.4 Methanogens and Methanotrophs

The archaeal sequencing reads mainly classified as taxa that contain methanogens in the phylum *Euryarchaeota*. The proportion of these reads generally increased with depth at all platforms (Figure 4-14) and read numbers were similar between 2016 and 2017. Sequences classified to genera associated with acetoclastic (*Methanosaeta)* and hydrogenotrophic (*Methanolinea, Methanoregula)* methanogenesis were identified in all FFT samples at similar proportions. The sequence read percentage for each of these three genera was low at the TWI (less than 2%) and maximum percentages were observed near the pit bottom (Figure 4-14). The percentage of sequencing reads classified to *Methanosaeta* increased to 6%. The read percentage for sequences classified to *Methanoregula* and *Methanolinea* increased to 8% and 4%, respectively. Finally, sequences classified to the genus *Candidatus Methanofastidiosum* were identified in all FFT samples at low percentages (less than 1%).

Reads classified to the class *Gammaproteobacteria* comprised a considerable proportion of the sequencing reads near the TWI (Figure 4-12) and included reads classified to several taxa capable of aerobic methanotrophy. Sequences classified to the genera *Methylobacter* and *Methyloparacoccus* comprised up to 5 and 8% of the total sequencing reads near the TWI, respectively. The proportion of these reads decreased greatly with depth. Sequences classified to *Methylobacter* were low (less than 1%) at depths greater than 1 m below the TWI and sequences classified to *Methyloparacoccus* were low (less than 1%) at depths greater than 5 m below the TWI. Sequences classified to taxa associated with anaerobic methane oxidation were also present in low proportions in the FFT deposit. Sequences classified to the NC10 phylum comprised up to 0.02% of the sequencing reads at scattered depths throughout the FFT. Microbes in this phylum are associated with NO_2-dependent anaerobic CH_4 oxidation (Ettwig et al., 2009). Sequences classified to the ANME-1 and ANME-2 groups associated with SO_4-dependent anaerobic CH_4 oxidation were not detected.

Figure 4-14: Stacked bar plot of archaeal reads as a portion of the total sequencing reads for August 2016 (A) and July 2017 (B). Sequencing reads for all samples have been subsampled to 34 200 reads.

CHAPTER 5: DISCUSSION

5.1 Depth-Dependent Trends in FFT Biogeochemistry

Distinct biogeochemical gradients were apparent across the interface between the water cap and underlying FFT deposit. The TWI depth increased from 2016 to 2017 due to FFT settlement and dewatering, which corresponds to pore-water expression and mass loading into the water cap (Dompierre et al., 2017). Dissolved SO_4 and pH were higher in the water cap relative to the FFT, whereas alkalinity, EC, $\sum H_2S$, NH_3-N and $CH_{4(aq)}$ exhibited the opposite trend. Microbial communities included an abundance of taxa commonly found in hydrocarbon-contaminated environments and the sequencing results suggest that hydrocarbons are a principal influence on biogeochemical processes. The microbial community exhibited the greatest metabolic diversity near the TWI and decreased with depth. The strong biogeochemical gradients and diverse microbial populations near the TWI indicate this zone may have important implications for mass loading during FFT settlement and dewatering.

The increased EC across the TWI can be correlated to increased Na^+, Cl^-, and HCO_3^- concentrations in the FFT pore water (Dompierre et al., 2016). The sharp pH decrease below the TWI is indicative of anaerobic microbial metabolisms in the FFT deposit (Siddique et al., 2014a). Hydrocarbon-degrading and fermenting microbes degrade carbon compounds in FFT and produce CO_2. Dissolved CO_2 in FFT pore water generates carbonic acid (H_2CO_3), a weak acid, which subsequently dissociates and decreases pH (Siddique et al., 2014a). The high-throughput amplicon sequencing results identified many microbes in the FFT samples that are likely capable of hydrocarbon degradation and produce CO_2. The *Anaerolineaceae* and *Peptococcaceae* families are associated with methanogenic hydrocarbon degradation (Liang et al., 2015; Tan et al., 2014) and sequences classified to these families were abundant in the FFT microbial communities (9 to 53% of total reads). Acetoclastic methanogens, SRB and other hydrocarbon degraders (eg., *Syntrophus* and *Smithella*) can also produce CO_2 in FFT deposits (Siddique et al., 2012). The slight differences in pH trends among platforms is attributed to the occurrence of different reactions that produce and consume CO_2. Additionally, CO_2 production and decreased pH is associated with the

observed increased alkalinity below the TWI. Dissolved CO_2 contributes to increased HCO_3^- when pore-water pH is above approximately 6.4 (Siddique et al., 2014a). Lower pH also promotes the dissolution of the carbonate minerals dolomite and calcite. This dissolution reaction releases divalent cations and increases HCO_3^- concentrations in FFT pore water (Dompierre et al., 2016; Siddique et al., 2014a).

Coupled geochemical and microbiological data further illustrate that a depth-dependent shift in biogeochemical processes occurs in the FFT deposit. Microbial diversity and species richness are highest directly below the TWI and the abundant families are associated with a variety of metabolisms relevant to the FFT pore-water chemistry. The deltaproteobacterial families *Desulfobulbaceae, Desulfobacteraceae* and *Syntrophaceae* are associated with SO_4 reduction and anaerobic hydrocarbon degradation (Foght et al., 2017). The *Methylococcaceae* family is associated with $CH_{4(aq)}$ oxidation (Saidi-Mehrabad et al., 2013) and the *Burkholderiaceae* family contains a metabolically diverse group of microbes. The upper 1.0 m of FFT below the TWI also contained the highest DNA concentrations, which is consistent with higher microbial density. Strong geochemical gradients were also exhibited in this zone and a variety of metabolic processes could be supported. Decreased pH directly below the TWI suggests CO_2 production and potential hydrocarbon degradation. Decreased SO_4 and increased $\sum H_2S$ concentrations within the upper 0.5 m of the FFT deposit indicates SO_4 reduction. Minimum NH_4^+ and $CH_{4(aq)}$ concentrations at the TWI suggests possible biological consumption processes within the upper few meters below the TWI.

The microbial diversity, species richness and geochemical variability decreases at depths greater than 5 m below the TWI. Hydrocarbon degradation and methanogenesis are the primary metabolic processes in the deeper FFT. The microbial community in this zone is dominated by taxa associated with hydrocarbon degradation, syntrophic metabolism and methanogenesis. The *Anaerolineaceae, Peptococcaceae, Methanoregulaceae, Methanosaetaceae* and *Syntrophaceae* families comprised 29 to 68% of the microbial community within this zone. The pH gradually decreased with depth due to CO_2 produced from hydrocarbon degradation and dissolved CH_4 concentrations were elevated throughout the FFT deposit. Dissolved SO_4 and $\sum H_2S$ were depleted at depths greater than 15 m below the TWI and total dissolved Fe concentrations approached the minimum detection limit by 20 m below the TWI.

As the FFT continues to settle and dewater, pore water will be expressed upward to the water cap and mass loading of dissolved constituents will occur across the TWI. Biogeochemical processes occurring throughout the FFT will impact the concentration of these dissolved constituents through production and consumption reactions as the pore water is expressed upwards. The biogeochemically dynamic zone immediately below the TWI likely has a substantial influence on pore-water concentrations and therefore strongly affects mass flux calculations and estimations of long-term mass loading to the water cap.

5.2 Biogeochemistry Near the Tailings-Water Interface

Nitrification, methanotrophy and $\sum H_2S$ oxidation were recently identified as O_2-consuming processes in the BML water cap (Risacher et al., 2018). The mass loading of dissolved NH_4^+, CH_4 and $\sum H_2S$ from the underlying FFT will therefore strongly affect oxygenation of the water cap. These dissolved constituents exhibited distinct depth-dependent trends and reached maximum values at different depths in the FFT deposit. However, the mass loading of these constituents will be strongly impacted near the TWI where a potential for biologically-driven reactions involving N, Fe, S and C species occurs.

Nitrification is an important control on NH_4^+ concentrations in the BML water cap (Risacher et al., 2018). This aerobic microbial process couples O_2 reduction with NH_4^+ oxidation to NO_2, which is then oxidized to NO_3 (Devol, 2015). Dissolved NH_4^+ concentrations in the FFT deposit decreased as pore water was expressed upward to the TWI and may be attributed to microbial NH_4^+ consumption. The NH_4^+-oxidizing microbe *Nitrosomonas* can perform the first step of nitrification and was present at the TWI at low sequence abundance (<1%). Aerobic nitrification in the FFT deposit is likely limited by O_2 availability; however, the species *Nitrosomonas eutropha* is capable of anammox (Ding et al., 2013), so it is possible that the *Nitrosomonas* in the tailings are performing this function. Although the presence of *Nitrosomonas* in the FFT deposit may also be due to preservation from the overlying water cap, there is some evidence that anammox processes may be occurring near the TWI. Anammox is a microbial process where NH_4^+ is anaerobically oxidized to nitrogen gas using NO_2 as the electron acceptor (Devol, 2015). Nitrogen mass loss relative to conservative ions suggests NH_4^+ concentrations may be influenced by anammox in the FFT deposit. The extent of N mass loss due to NH_4^+ ion exchange at clay mineral surfaces is poorly constrained, but the substantially higher Na^+ concentrations in

FFT pore water are expected to limit the extent of NH_4^+ exchange. Traditional anammox processes in FFT may be limited by the low NO_2 concentrations in FFT pore water. Any available NO_2 in the FFT pore water would likely be immediately consumed and therefore would not accumulate. Although sequences classified to the order *Planctomycetales* were present at the TWI, the candidate genera for traditional anammox were absent from the high-throughput amplicon sequencing data. However, anammox is also linked to the S and Fe biogeochemical cycles in marine and terrestrial systems (Bao and Li, 2017; Rios-Del Toro et al., 2018). The microbial taxa specific to these processes are poorly understood, however the presence of SO_4 and Fe(III) hydroxides near the TWI suggest the potential for this process to occur at shallow depths in the FFT deposit.

Aerobic methane oxidation, or methanotrophy, is a key O_2-consuming process in the BML water cap (Risacher et al., 2018). Aerobic methanotrophs, specifically the gammaproteobacterial *Methyloparacoccus* and *Methylobacter*, comprised a relatively large proportion of the sequencing reads (4 to 9%) directly below the TWI. Although aerobic methanotrophy is unlikely to be a main CH_4-consuming process in the FFT, aerobic methanotrophs belonging to the class *Gammaproteobacteria* were recently found to be active under anoxic conditions in lake systems (Martinez-Cruz et al., 2017; Oswald et al., 2016). Although the exact mechanisms of this activity are not well understood, it is proposed that processes occurring in anoxic sediments may provide trace O_2 concentrations that can be consumed by aerobic methanotrophs. Dissolved O_2 in the BML water cap was detected at the TWI in Summer 2016 (Risacher et al., 2018), and low O_2 concentrations at the TWI may be rapidly consumed by these microbes. A proportion of the sequences corresponding to the taxa *Methyloparacoccus* and *Methylobacter* may also be due to cells that had settled in the FFT from the water cap.

Evidence from the geochemical data suggests mass transfer reactions involving $CH_{4(aq)}$ likely occurred near the TWI. Within the upper 2 m of the FFT deposit, $CH_{4(aq)}$ concentrations decreased from 40 mg L^{-1} to approximately zero in the water cap. This decrease may be attributed to microbially-driven anaerobic methane oxidation. The high-throughput amplicon sequencing data identified low proportions (<0.02%) of microbes belonging to the NC10 phylum. Members of this phylum are capable of anaerobic CH_4 oxidation coupled to NO_3 or NO_2 reduction (Ettwig et al., 2009). The very low proportions of these microbes in the FFT deposit suggest that

this process is likely limited by NO_3 and NO_2 availability in the FFT pore water. Specific SO_4-utilizing ANME taxa were not identified in the sequencing data. However, sequences of SRB taxa associated with ANME-1 and ANME-2 groups, *Desulfosarcina* and *Desulfococcus,* were detected in low percentages (<0.1%) (Knittel and Boetius, 2009). Sulfate-dependent $CH_{4(aq)}$ oxidation in the FFT deposit would likely be restricted to a short depth interval near the TWI where O_2 is limited and SO_4 is available. Microbial aerobic and anaerobic CH_4 oxidation processes in the FFT deposit have the potential to greatly decrease the $CH_{4(aq)}$ flux across the TWI and should be considered in long-term CH_4 mass flux calculations.

Past studies identified an Fe-reducing zone directly below the TWI, where precipitation of Fe(II)-sulfide phases is an important control on dissolved Fe and $\sum H_2S$ concentrations (Dompierre et al., 2016; Stasik et al., 2014). This process can greatly decrease $\sum H_2S$ mass loading to the water cap and geochemical modeling supports the interpretation of $FeS_{(s)}$ precipitation under SO_4-reducing conditions (Dompierre et al., 2016). Sequences classified to the Fe-reducing genera *Rhodoferax* were detected in high proportions (2 to 13%) at the TWI, which suggests that microbial Fe reduction may be active in this zone. An increase in pore-water Fe concentrations directly below the TWI was not observed in 2016 or 2017, but it is likely that any Fe(II) produced near the TWI was quickly precipitated as Fe(II)-sulfide minerals. The *Desulfobulbaceae* family is also associated with the formation of amorphous Fe(II)-sulfide minerals in fine tailings (Siddique et al., 2014b) and was present in high sequence read percentages throughout the FFT deposit (Figure 4-13). Sequences classified as *Rhodoferax* were present throughout the FFT deposit and total dissolved Fe concentrations gradually increased in the FFT below the zone of SO_4 reduction. This increase was likely due to the lack of abiotic sulfide mineral precipitation reactions because of limited $\sum H_2S$ concentrations.

5.3 Dominant Biogeochemical Processes in FFT

5.3.1 Sulfur Cycling

Sulfate reduction was a main electron-accepting process in the FFT deposit, likely sustained by the elevated SO_4 concentrations in the water cap (Dompierre et al., 2016; Risacher et al., 2018). Sulfate reduction occurs within the upper 0.5 m of FFT, where a sharp decrease in SO_4 concentrations and corresponding increase in dissolved $\sum H_2S$ occur. This zone is also

characterized by the presence of sequencing reads classified as SRB-associated taxa, which comprised an average of 12 ± 4% (*n*=24) of the sequencing reads. These sequences primarily classified as *Desulfoprunum* and isolates of this genus can couple SO_4 reduction with the complete oxidation of various short-chain fatty acids (Junghare and Schink, 2015). Unclassified genera belonging to the *Desulfobulbaceae* and *Desulfobacteraceae* families were also abundant directly below the interface (Figure 4-13). These families are capable of coupling SO_4 reduction with hydrocarbon degradation (Foght et al., 2017; Mohamad Shahimin et al., 2016). Many known SRB contain multiple copies of the 16S rRNA gene. For instance, isolates within the family *Desulfobulbaceae* can contain between two and seven 16S rRNA gene copies (Stoddard et al., 2015). The proportion of SRB identified by sequencing reads in the FFT deposit may therefore be overestimated. However, correcting for 16S rRNA gene copy numbers was not conducted, as exact copy numbers were not known for all SRB and inaccurate predictions can further skew proportions in the community profile (Louca et al., 2018). Sulfate reduction will likely remain an important process at the TWI while SO_4 remains elevated in the overlying water cap. It is important to monitor SO_4 reduction directly below the TWI because the $\sum H_2S$ flux to the water cap can impact O_2 concentrations and water quality. The $\sum H_2S$ concentrations directly above the TWI were low (<50 µg L^{-1}) and when O_2 persists to the TWI these concentrations are completely oxidized in the hypolimnion (Risacher et al., 2018). However, dissolved $\sum H_2S$ has the potential to remain in the water cap if O_2 ceases to persist to the TWI.

Sulfur reduction also occurred at deeper depths in the FFT deposit, since elevated $\sum H_2S$ concentrations were observed down to 15 m below the TWI. The proportion of sequencing reads classified as SRB taxa or taxa associated with SOI reduction/disproportionation also remained generally consistent to this depth (Figure 4-13). The use of SO_4 as an electron acceptor likely decreased with depth, due to its low availability below the interface. However, the proportion of SOIs in the total S pool greatly increased with depth (Figure 4-7), comprising over 55% of the pool at depths greater than 5.0 m below the TWI. Although all SRB can utilize SO_4 as an electron acceptor, some microbes detected in the FFT are also capable of SOI reduction or disproportionation reactions. *Desulfatirhabdium* and *Desulfatitalea* use both SO_4 and thiosulfate (S_2O_3) as electron acceptors and taxa classified as these genera were consistently present throughout the FFT deposit (Balk et al., 2008; Higashioka et al., 2013). The *Desulfobulbaceae* family includes microbes that grow by S disproportionation, plus taxa involved in anaerobic

hydrocarbon degradation (Foght et al., 2017; Milucka et al., 2012). The genera *Desulfurivibrio* and *Desulfocapsa* grow by disproportionation of elemental S, resulting in the production of both SO_4 and $\sum H_2S$ (Finster et al., 2013; Poser et al., 2013). Although the proportion of *Desulfocapsa* remained relatively low (<1.0%) throughout the FFT deposit, *Desulfurivibrio* was present in high sequence percentages (1 to 10%) in deeper depths at Platforms 1 and 3. The increased $\sum H_2S$ at depths with low SO_4 concentrations indicates that SOIs likely have an important role in S biogeochemistry within the FFT deposit. This finding has implications for S mass balance calculations within BML.

Sequences classified as the SOI-oxidizing taxa *Sulfuritalea* and *Sulfurimonas* were identified near the TWI. These microbes are facultative anaerobes that can couple SOI oxidation with nitrogen reduction. *Sulfuritalea* can oxidize thiosulfate, elemental S, and H_2 using NO_3 as an electron acceptor (Kojima and Fukui, 2011). *Sulfurimonas* can also couple the oxidation of elemental S or H_2 with denitrification (Sievert et al., 2008). These metabolisms would likely be limited by NO_3 availability in the FFT deposit. Anaerobic SOI oxidation likely plays a small role in the overall S cycle, however it has the potential to influence the mass transport of S species across the TWI.

5.3.2 Carbon Cycling

Overall, the sequencing reads were largely comprised of hydrocarbon-degrading and other fermenting microbes. These microbes were present throughout the FFT deposit and the proportion of taxa associated with hydrocarbon degradation generally increased with depth (Figure 4-12). The hydrocarbon degraders identified from the sequencing results are closely related to organisms that can break down various components found in naphtha, including some *n*-alkanes and BTEX compounds. The *Anaerolineaceae, Peptococcaceae, Syntrophaceae* and *Desulfobacteraceae* families can degrade *n*-alkanes, producing CH_3COO^- that can then be used by acetoclastic methanogens (Mohamad Shahimin et al., 2016). Together these families comprised 30 to 59% of the sequencing reads at depths greater than 1 m below the TWI. The syntrophic microbes *Syntrophus* and *Smithella,* belonging to the *Syntrophaceae* family, produce CH_3COO^-, H_2 and CO_2, and are commonly reported as crucial participants in methanogenic hydrocarbon degradation (Foght et al., 2017; Siddique et al., 2012). The large proportion of these families in deeper FFT samples suggest that hydrocarbon degradation is an important process at depth and plays a central

role in providing substrates to support methanogenesis. Hydrocarbon degradation may be the rate-limiting step for various microbial metabolisms, including methanogenesis. Other microbes capable of organic carbon degradation were present throughout the FFT and can completely oxidize organic compounds to CO_2, or incompletely oxidize them to form organic acids, such as formate, pyruvate and CH_3COO^-. Many SRB can ferment organic acids in the absence of SO_4, producing H_2, CO_2 and CH_3COO^- (Plugge et al., 2011). Sequences affiliated with the H_2-consuming microbe *Hydrogenophaga* were present in low sequence abundance (<1.0%) throughout the FFT. This genus and other H_2-consuming microbes usually grow in a syntrophic relationship with fermenting microbes (Plugge et al., 2011). The incomplete oxidation of organic carbon compounds in FFT can provide a wide range of substrates for microbes to consume to drive their metabolisms.

Methanogenesis was an active and important process in the FFT deposit. The $CH_{4(aq)}$ concentrations were above 30 mg L^{-1} at depths as shallow as 1 m below the TWI (Figure 4-8) and 2017 data indicates concentrations were elevated throughout the FFT deposit. The proportion of Archaea corresponding to methanogenic taxa generally increased with depth, comprising 10 to 19% of the sequencing reads in the deepest FFT samples. Acetoclastic and hydrogenotrophic methanogens were present throughout the FFT profile in similar proportions (Figure 4-14). Methane can therefore potentially be produced through CH_3COO^- fermentation and CO_2 reduction pathways in BML. Laboratory experiments examining methanogenic hydrocarbon degradation in fine tailings have identified the occurrence of both acetoclastic and hydrogenotrophic methanogenesis (Siddique et al., 2012; Stasik and Wendt-Potthoff, 2016). Research examining carbon isotope fractionation suggests that the preferred pathway for CH_4 production in BML is acetoclastic methanogenesis (Goad, 2017). Long-term CH_4 production in FFT will be largely dependent on the available substrates for methanogens. Over time, labile carbon sources will become depleted and CH_3COO^- availability will likely be controlled by *in situ* hydrocarbon degradation. However, hydrogenotrophic methanogens could still consume H_2 and CO_2, which are produced from various fermentative metabolisms. Furthermore, the proportion of sequence reads classified to methanogenic taxa in BML was 1 to 2 orders of magnitude higher than reads reported in an oil sands tailings study involving SO_4-rich centrifuged fine tailings (Heaton, 2015). The high proportion of methanogenic taxa in BML is likely due to the greater availability of substrates produced by anaerobic hydrocarbon-degrading microbes that consume the residual naphtha in FFT

(Siddique et al., 2007). Methanogenesis will likely be an important process to monitor in any future EPLs containing FFT with residual naphtha.

5.4 Conceptual Model for FFT Biogeochemistry

The conceptual model for FFT biogeochemistry can be used as a tool to identify relationships between the N, Fe, S and C biogeochemical cycles in FFT and predict how biologically-driven reactions can impact long-term mass loading across the TWI. Collaborative research examining BML pore-water chemistry, mineralogy, microbiology and reactive transport modelling is contributing to the ongoing development of the overall conceptual model for FFT biogeochemistry (Figure 1-1). The basis of the conceptual model is focused on the upward expression of FFT pore water due to the settlement and dewatering of tailings. The dominant chemical mass transport process during early stage development of BML is advection-dispersion driven by tailings settlement (Dompierre et al., 2017). The FFT pore water contains dissolved salts, NH_4^+, $\sum H_2S$ and CH_4, and long-term mass loading of these constituents across the TWI can impact the development of an oxic water cap with adequate water quality standards. Although the FFT settlement rate will decrease over time, pore-water expression and diffusion of these chemical constituents to the water cap will remain an important influence in the long-term development of a self-sustaining EPL. This thesis contributes to the overall conceptual model by examining the depth-related influences of biological processes on FFT pore-water chemistry to inform predictions on long-term chemical mass loading.

The microbes identified in the FFT deposit can drive reactions which alter the concentrations of dissolved N, Fe, S and C species. The importance of these biogeochemical processes in terms of chemical mass loading shifts with depth (Figure 5-1). Throughout the FFT deposit, hydrocarbon degradation and fermentative processes produce substrates that can support a variety of heterotrophic processes. Dissolved NH_4^+, $\sum H_2S$ and $CH_{4(aq)}$ concentrations can be elevated at depths greater than 1.5 m below the TWI from biotic and abiotic reactions (Figure 5-1). As pore water is expressed up towards the water cap, the concentrations of these constituents are affected through reactions occurring in a biogeochemically-dynamic zone directly below the TWI. Physical mixing at the TWI by CH_4 ebullition or other processes may enhance downward transport of SO_4 and O_2 from the water cap into the upper FFT (Figure 5-1). Biologically-driven reactions

occurring in this upper FFT zone can potentially decrease the long-term chemical mass loading of NH_4^+, $\sum H_2S$ and $CH_{4(aq)}$ across the TWI, which has important implications for water cap quality.

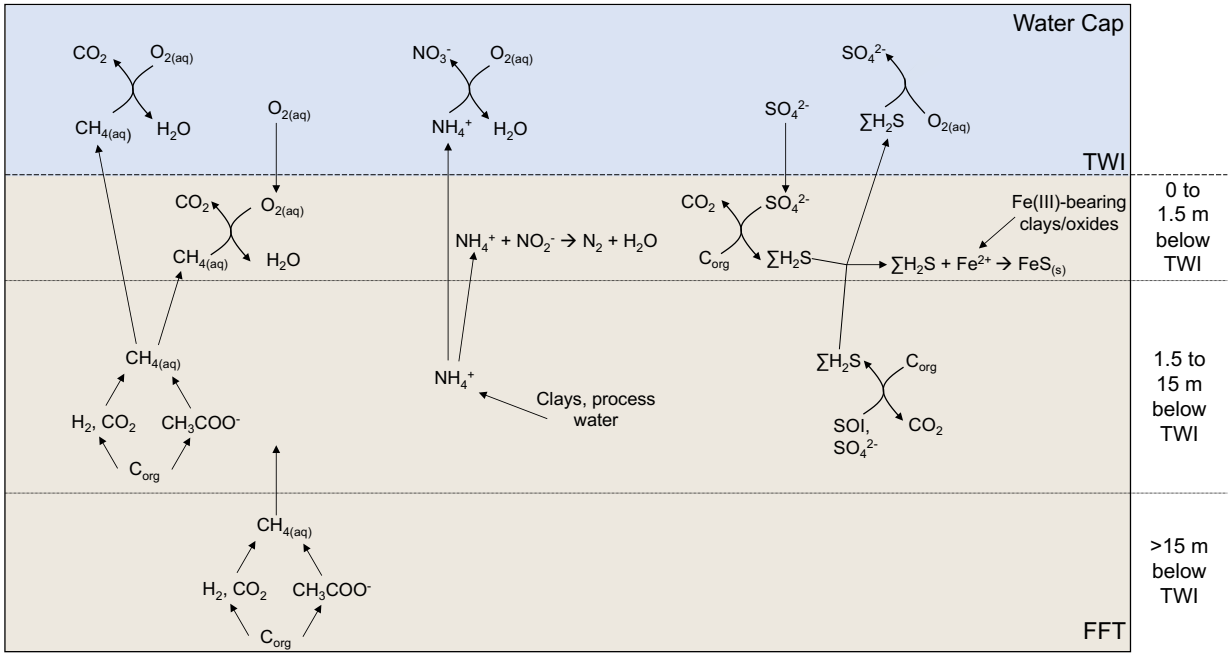

Figure 5-1: General conceptual figure demonstrating the overall zonation of biogeochemical processes in the FFT deposit.

The elevated NH_4^+ concentrations in deeper FFT could potentially be due to high concentrations typically present in process-affected waters (Allen, 2008). It may also be due to NH_4^+ released from clay mineral surfaces, however NH_4^+ ion exchange in FFT is poorly constrained. This fixed mass source is important to consider for predicting long-term NH_4^+ mass loading because it may eventually become depleted over time. Long-term NH_4^+ mass loading can also be affected by reactions occurring in the dynamic zone directly below the TWI. As dissolved NH_4^+ is expressed upwards it may be oxidized to N_2 gas via anammox processes (Figure 5-1). Dissolved NH_4^+ that is not oxidized in the FFT will be expressed across the TWI and into the water cap. In the water cap, it is oxidized to NO_3 via nitrification when O_2 is available (Risacher et al., 2018). It is important to note that the oxidation reactions that can occur in the water cap (Figure 5-1) are dependent on O_2 and if this constituent is absent from the deep cap waters there is potential for NH_4^+, $\sum H_2S$ and $CH_{4(aq)}$ concentrations to become elevated in the shallower zones.

Labile organic acids and H_2 produced from the degradation of organic C can be consumed by SRB and SOI-reducing microbes to produce $\sum H_2S$ in the upper 15 m of the FFT deposit. The $\sum H_2S$ produced in deeper FFT may be attributed to SOI reduction or disproportionation reactions because there is not a constant SO_4 source in this zone. The increased $\sum H_2S$ concentrations directly below the TWI were likely due to microbial SO_4 reduction. The source of SO_4 is from the process-affected water in the overlying water cap. Over time, the importance of SO_4 reduction at the TWI may decrease because the cap water will gradually be replaced with fresh water from the Beaver Creek Reservoir. When $\sum H_2S$ is present in the biochemically active zone directly below the TWI it can potentially combine with Fe^{2+} to form the Fe(II)-sulfide minerals FeS or FeS_2 (Figure 5-1). This reaction may control long-term $\sum H_2S$ mass loading across the TWI. The source of dissolved Fe^{2+} to the system is likely Fe(III)-bearing oxides from the water cap or, potentially, structural Fe(III) in FFT clay minerals. Changes in mass fluxes would be expected if the availability of dissolved $\sum H_2S$ or Fe^{2+} changes with time. In the absence of Fe^{2+}, $\sum H_2S$ may be expressed across the TWI and into the water cap where oxidation to SO_4 would occur in the presence of O_2.

Dissolved CH_4 is produced throughout the deeper FFT zones and methanogenesis may occur at depths as shallow as 1.5 m below the TWI. Methanogenesis can occur via two pathways in the FFT deposit (Figure 5-1) and long-term production will, therefore, be controlled by the availability of CH_3COO^-, CO_2 and H_2 produced by syntrophic microbes. Although rates will likely vary both spatially and temporally, methanogenesis could potentially continue for a long period of time. Additionally, dissolved CH_4 may be oxidized by aerobic and anaerobic microbial processes in the shallow FFT zone directly below the TWI (Figure 5-1). Aerobic $CH_{4(aq)}$ oxidation is dependent on the presence of O_2 and this constituent may occasionally be present in low concentrations directly below the TWI from physical mixing processes. Anaerobic $CH_{4(aq)}$ oxidation will be limited by the availability of NO_3 and NO_2 in the FFT pore water. Dissolved $CH_{4(aq)}$ that is not oxidized in the shallow FFT zone is further expressed upward across the TWI and can be oxidized to CO_2 in the water cap when O_2 is present.

These results have helped refine the overall conceptual model (Figure 1-1) through the addition of depth information, N biogeochemistry and providing taxonomic information of the microbes present. Analysis of the depth-dependent relationships between FFT microbial community structure and pore-water chemistry identified major zones where concentrations of

dissolved NH_4^+, $\sum H_2S$ and CH_4 are affected by microbially-driven processes. This finding has important implications for predicting long-term mass loading because it provides a greater understanding of how the concentrations of these constituents can be influenced directly below the TWI. In addition, the microbes identified in the FFT support the assumptions made in the overall conceptual model (Figure 1-1) that SRB and methanogens are prominent members of the microbial community and exert a strong influence on pore-water chemistry. However, the microbiological analysis also identified microbes that were not initially expected to be present or play a large role in influencing FFT biogeochemistry. This included microbes associated with SOI reduction/disproportionation and aerobic/anaerobic CH_4 oxidation.

CHAPTER 6: CONCLUSIONS AND FUTURE RECOMMENDATIONS

6.1 Conclusions

The overall goal of this research was to develop an understanding of the relationships between microbiology and pore-water chemistry in the FFT deposit of the first full-scale demonstration EPL. High-throughput amplicon sequencing was used to identify the spatial distribution of microbial taxa and a detailed analysis of pore-water chemistry was used to identify geochemical gradients of dissolved N, Fe, S and C species. The microbiological and geochemical data was used to identify how microbial processes impact pore-water chemistry and the mass transfer of dissolved constituents across the TWI. This research identified distinct depth-dependent trends in pore-water chemistry and microbial community structure in the FFT deposit. It was also determined that anaerobic microbial processes occurring in the FFT can control pore-water pH, as well as the abundance and distribution of N, Fe, S and C species within the FFT and across the TWI. Together, these findings refined the conceptual model to better understand the relationship between biogeochemical cycles in the FFT deposit and predict long-term mass loading of dissolved species to the water cap.

Microbial diversity in the FFT deposit was highest directly below the TWI and biogeochemical processes occurring in this dynamic zone can potentially reduce the long-term flux of $\sum H_2S$, $CH_{4(aq)}$ and NH_4^+ across the TWI. Anaerobic hydrocarbon degradation and various other anaerobic microbial processes occurring below the TWI produced CO_2, resulting in decreased pore-water pH below the TWI. A zone of SO_4 reduction occurred directly below the TWI and $\sum H_2S$ concentrations increased to values over 1 mg L^{-1} within the upper 3 m of the FFT deposit. Sequences classified as SRB-associated taxa were abundant (12 ± 4%) in this zone and were primarily classified as *Desulfoprunum, Desulfobulbaceae* and *Desulfobacteraceae*. Secondary sulfide mineral precipitation reactions occurring near the TWI likely decreased $\sum H_2S$ mass transport to the water cap. Sequences classified to the aerobic CH_4-oxidizing genera *Methyloparacoccus* and *Methylobacter*, as well as the anaerobic CH_4-oxidizing phylum NC10,

were present at the TWI. Dissolved CH_4 concentrations in this zone were low (<10 mg L^{-1}) compared to deeper FFT samples (>30 mg L^{-1}), suggesting the occurrence of biologically-driven $CH_{4(aq)}$ oxidation reactions. Finally, biologically-driven NH_4^+ oxidation reactions potentially occurred near the TWI, since N mass loss occurred in this zone and minimum values for pore-water NH_4^+ concentrations were observed at the TWI.

Hydrocarbon degradation and methanogenesis were the primary metabolic processes in deeper FFT. The microbial taxa at depths greater than 5 m below the TWI was dominated by the *Anaerolineaceae, Peptococcaceae, Methanoregulaceae, Methanosaetaceae* and *Syntrophaceae* families. Pore-water pH gradually decreased in this zone and $CH_{4(aq)}$ concentrations remained above 30 mg L^{-1}. Microbial CH_4 production was likely sustained by hydrocarbon degradation from syntrophic microbes and the primary methanogenic pathway may change over time as labile carbon sources become depleted and CH_3COO^- availability is controlled by hydrocarbon degradation. Reactions involving SOI reduction and disproportionation also likely occurred in deeper FFT. Species such as elemental S and thiosulfate may have a large role in the S biogeochemical cycle and are important to consider in long-term S mass balance calculations. The findings from this thesis can provide insight for future EPL development, however, further biogeochemical studies should be conducted for EPLs containing different tailings materials. The findings from this thesis can have relevance to other hydrocarbon-contaminated sites and other anaerobic systems where there is an intricate relationship between carbon degradation and the biogeochemical cycles of N, Fe, S and C.

6.2 Recommendations for Future Studies

Findings from this thesis demonstrate that FFT biogeochemistry did not vary substantially over the two-year study period and may not need to be monitored annually. Monitoring of pore-water chemistry could be limited to years where chemical data from the water cap suggest that biogeochemical processes occurring in the FFT deposit may be changing.

Further studies examining FFT microbiology can identify the presence of relevant genes and the activity of potentially important microbes identified from the high-throughput amplicon sequencing data. Shotgun metagenomic sequencing could be used to identify the presence of genes belonging to functionally-relevant microbes. For instance, this technique may identify the presence

of genes associated with anammox and anaerobic methane oxidation processes. Quantitative PCR is used to obtain an estimation of gene copy numbers and could be used to quantitatively examine how the copy numbers of a specific gene changes with depth in the FFT deposit. This analysis could be used to quantify the abundance of the *dsrA* gene associated with dissimilatory SO_4 reduction and the *mcrA* gene associated with methanogenesis. Finally, phospholipid fatty acid analyses could identify whether the aerobic methanotrophs present near the TWI are utilizing the carbon in CH_4 for assimilatory processes.

Further examination of FFT chemistry can provide a better understanding of relevant geochemical processes identified in this thesis. Analysis of the distribution and abundance of individual SOI species in the FFT deposit, specifically elemental S and thiosulfate, would identify which S species have the greatest influence on the S cycle in the FFT. Isotope tracer experiments utilizing ^{15}N-labelled NO_3, NO_2 and NH_4^+ can also be used to examine the occurrence of anammox in the FFT deposit. Further research examining solid-phase FFT mineralogy can provide greater insight into the occurrence of Fe(II)-sulfide mineral precipitation reactions directly below the TWI.

REFERENCES

Alberta Energy Regulator (2017a). Directive 085: Fluid tailings management for oil sands mining projects. Alberta Energy Regulator, Calgary, AB.

Alberta Energy Regulator (2017b). Suncor Energy Inc. Applications for Millennium operational amendment and Base Plant tailings management plan. Alberta Energy Regulator, Calgary, AB.

Alberta Environment and Parks (2015). Mineable oil sands fluid tailings volume by facility as of the end of 2013. *Oil Sands Information Portal, Alberta Environment and Parks*. Edmonton, AB. Available at: http://osip.alberta.ca/library/Dataset/Details/540.

Alberta Environment and Parks (2017). Oil sands mines reclamation and disturbance tracking by company to the end of the reporting year. *Oil Sands Information Portal, Alberta Environment and Parks*. Edmonton, AB. Available at: http://osip.alberta.ca/library/Dataset/Details/29.

Alberta Government (2015). Lower Athabasca region tailings management framework for the mineable Athabasca oil sands. Alberta Government, Edmonton, AB.

Alberta Government (2017). Alberta oil sands industry quarterly update: Winter 2017. Alberta Government, Edmonton, AB.

Allen, E. W. (2008). Process water treatment in Canada's oil sands industry: I. Target pollutants and treatment objectives. *Journal of Environmental Engineering and Science* 7, 499–524. doi:10.1139/S08-020.

Balk, M., Altinbaş, M., Rijpstra, W. I. C., Damsté, J. S. S., and Stams, A. J. M. (2008). Desulfatirhabdium butyrativorans gen. nov., sp. nov., a butyrate-oxidizing, sulfate-reducing bacterium isolated from an anaerobic bioreactor. *International Journal of Systematic and Evolutionary Microbiology* 58, 110–115. doi:10.1099/ijs.0.65396-0.

Bao, P., and Li, G. X. (2017). Sulfur-driven iron reduction coupled to anaerobic ammonium oxidation. *Environmental Science and Technology* 51, 6691–6698. doi:10.1021/acs.est.6b05971.

Beal, E. J., House, C. H., and Orphan, V. J. (2009). Manganese- and iron- dependent marine

methane oxidation. *Science* 325, 184–187. doi:10.1126/science.1169984.

Bethke, C. M., Ding, D., Jin, Q., and Sanford, R. A. (2008). Origin of microbiological zoning in groundwater flows. *Geology* 36, 739–742. doi:10.1130/G24859A.1.

Bethke, C. M., Sanford, R. A., Kirk, M. F., Jin, Q., and Flynn, T. M. (2011). The thermodynamic ladder in geomicrobiology. *American Journal of Science* 311, 183–210. doi:10.2475/03.2011.01.

Chalaturnyk, R. J., Scott, J. D., and Özüm, B. (2002). Management of oil sands tailings. *Petroleum Science and Technology* 20, 1025–1046. doi:10.1081/LFT-120003695.

Champ, D. R., Gulens, J., and Jackson, R. E. (1979). Oxidation-reduction sequences in groundwater flow systems. *Canadian Journal of Earth Sciences* 16, 12–23.

Chapelle, F. H., and Lovley, D. R. (1992). Competitive exclusion of sulfate reduction by Fe(III)-reducing bacteria: a mechanism for producing discrete zones of high-iron ground water. *Groundwater* 30, 29–36.

Chen, M., Walshe, G., Chi Fru, E., Ciborowski, J. J. H., and Weisener, C. G. (2013). Microcosm assessment of the biogeochemical development of sulfur and oxygen in oil sands fluid fine tailings. *Applied Geochemistry* 37, 1–11. doi:10.1016/j.apgeochem.2013.06.007.

COSIA (2012). Technical guide for fluid fine tailings management. Canada's Oil Sands Innovation Alliance Inc.

Devol, A. H. (2015). Denitrification, anammox, and N_2 production in marine sediments. *Annual Review of Marine Science* 7, 403–423. doi:10.1146/annurev-marine-010213-135040.

Ding, S., Zheng, P., Lu, H., Chen, J., Mahmood, Q., and Abbas, G. (2013). Ecological characteristics of anaerobic ammonia oxidizing bacteria. *Applied Microbiology and Biotechnology* 97, 1841–1849. doi:10.1007/s00253-013-4697-0.

Dompierre, K. A., and Barbour, S. L. (2016). Characterization of physical mass transport through oil sands fluid fine tailings in an end pit lake: a multi-tracer study. *Journal of Contaminant Hydrology* 189, 12–26. doi:10.1016/j.jconhyd.2016.03.006.

Dompierre, K. A., Barbour, S. L., North, R. L., Carey, S. K., and Lindsay, M. B. J. (2017).

Chemical mass transport between fluid fine tailings and the overlying water cover of an oil sands end pit lake. *Water Resources Research* 53, 1–16. doi:10.1002/2016WR020112.

Dompierre, K. A., Lindsay, M. B. J., Cruz-Hernández, P., and Halferdahl, G. M. (2016). Initial geochemical characteristics of fluid fine tailings in an oil sands end pit lake. *Science of the Total Environment* 556, 196–206. doi:10.1016/j.scitotenv.2016.03.002.

Dong, H., Kukkadapu, R. K., Fredrickson, J. K., Zachara, J. M., Kennedy, D. W., and Kostandarithes, H. M. (2003). Microbial reduction of structural Fe(III) in illite and goethite. *Environmental Science and Technology* 37, 1268–1276. doi:10.1021/es020919d.

Ettwig, K. F., Butler, M. K., Le Paslier, D., Pelletier, E., Mangenot, S., Kuypers, M. M. M., et al. (2010). Nitrite-driven anaerobic methane oxidation by oxygenic bacteria. *Nature* 464, 543–548. doi:10.1038/nature08883.

Ettwig, K. F., Van Alen, T., Van De Pas-Schoonen, K. T., Jetten, M. S. M., and Strous, M. (2009). Enrichment and molecular detection of denitrifying methanotrophic bacteria of the NC10 phylum. *Applied and Environmental Microbiology* 75, 3656–3662. doi:10.1128/AEM.00067-09.

Fedorak, P. M., Coy, D. L., Salloum, M. J., and Dudas, M. J. (2002). Methanogenic potential of tailings samples from oil sands extraction plants. *Canadian Journal of Microbiology* 48, 21–33.

Findlay, A. J., and Kamyshny, A. (2017). Turnover rates of intermediate sulfur species (S_x^{2-}, S^0, $S_2O_3^{2-}$, $S_4O_6^{2-}$, SO_3^{2-}) in anoxic freshwater and sediments. *Frontiers in Microbiology* 8, 1-15. doi:10.3389/fmicb.2017.02551.

Finster, K. W., Kjeldsen, K. U., Kube, M., Reinhardt, R., Mussmann, M., Amann, R., et al. (2013). Complete genome sequence of desulfocapsa sulfexigens, a marine deltaproteobacterium specialized in disproportionating inorganic sulfur compounds. *Standards in Genomic Sciences* 8, 58–68. doi:10.4056/sigs.3777412.

Flynn, T. M., Loughlin, E. J. O., Mishra, B., Dichristina, T. J., and Kemner, K. M. (2014). Sulfur-mediated electron shuttling during bacterial iron reduction. *Science* 344, 1039–1042. doi:10.1126/science.1252066.

Foght, J. M., Gieg, L. M., and Siddique, T. (2017). The microbiology of oil sands tailings: past, present, future. *FEMS Microbiology Ecology* 93, 1–22. doi:10.1093/femsec/fix03.

Goad, C. (2017). Methane biogeochemical cycling over seasonal and annual scales. M.Sc. Thesis, McMaster University, Hamilton, Canada, 116 pp.

Government of Alberta (2009). Environmental management of Alberta's oil sands. Government of Alberta, Edmonton AB.

HACH Method 10205 (2016). Nitrogen-Ammonium, Salicylate TNTplus Method.

HACH Method 8131 (2015). Sulfide USEPA Methylene Blue Method.

Heaton, K. (2015). Biogeochemical investigation of centrifuged fine tailings deposits at an oil sands mine in Northern Alberta, Canada. M.Sc. Thesis, University of Saskatchewan, Saskatoon, Canada, 144 pp.

Higashioka, Y., Kojima, H., Watanabe, M., and Fukui, M. (2013). Desulfatitalea tepidiphila gen. nov., sp. nov., a sulfate-reducing bacterium isolated from tidal flat sediment. *International Journal of Systematic and Evolutionary Microbiology* 63, 761–765. doi:10.1099/ijs.0.043356-0.

Holowenko, F. M., MacKinnon, M. D., and Fedorak, P. M. (2000). Methanogens and sulfate-reducing bacteria in oil sands fine tailings waste. *Canadian Journal of Microbiology* 46, 927–937.

Illumina (2013). 16S Metagenomic Sequencing Library Preparation.

Jin, Q., and Kirk, M. F. (2018). pH as a primary control in environmental microbiology: 1. Thermodynamic perspective. *Frontiers in Environmental Science* 6, 1-15. doi:10.3389/FENVS.2018.00021.

Junghare, M., and Schink, B. (2015). Desulfoprunum benzoelyticum gen. nov., sp. nov., a gram-stain-negative, benzoate-degrading, sulfate-reducing bacterium isolated from a wastewater treatment plant. *International Journal of Systematic and Evolutionary Microbiology* 65, 77–84. doi:10.1099/ijs.0.066761-0.

Kasperski, K. L., and Mikula, R. J. (2011). Waste streams of mined oil sands: characteristics and

remediation. *Elements* 7, 387–392. doi:10.2113/gselements.7.6.387.

Knittel, K., and Boetius, A. (2009). Anaerobic oxidation of methane: progress with an unknown process. *Annual Review of Microbiology* 63, 311–334. doi:10.1146/annurev.micro.61.080706.093130.

Kojima, H., and Fukui, M. (2011). Sulfuritalea hydrogenivorans gen. nov., sp. nov., a facultative autotroph isolated from a freshwater lake. *International Journal of Systematic and Evolutionary Microbiology* 61, 1651–1655. doi:10.1099/ijs.0.024968-0.

Kozich, J. J., Westcott, S. L., Baxter, N. T., Highlander, S. K., and Schloss, P. D. (2013). Development of a dual-index sequencing strategy and curation pipeline for analyzing amplicon sequence data on the MiSeq Illumina sequencing platform. *Applied and Environmental Microbiology* 79, 5112–5120. doi:10.1128/AEM.01043-13.

Liang, B., Wang, L. Y., Mbadinga, S. M., Liu, J. F., Yang, S. Z., Gu, J. D., et al. (2015). Anaerolineaceae and Methanosaeta turned to be the dominant microorganisms in alkanes-dependent methanogenic culture after long-term of incubation. *AMB Express* 5, 1–13. doi:10.1186/s13568-015-0117-4.

Light, T. S. (1972). Standard solution for redox potential measurements. *Analytical Chemistry* 44, 1038–1039. doi:10.1021/ac60314a021.

Liu, Y., and Whitman, W. B. (2008). Metabolic, phylogenetic, and ecological diversity of the methanogenic archaea. *Annals of the New York Academy of Sciences* 1125, 171–189. doi:10.1196/annals.1419.019.

Louca, S., Doebeli, M., and Parfrey, L. W. (2018). Correcting for 16S rRNA gene copy numbers in microbiome surveys remains an unsolved problem. *Microbiome* 6, 1–12. doi:10.1186/s40168-018-0420-9.

Luo, J., Chen, H., Hu, S., Cai, C., Yuan, Z., and Guo, J. (2018). Microbial selenate reduction driven by a denitrifying anaerobic methane oxidation biofilm. *Environmental Science & Technology* 52, 4006–4012. doi:10.1021/acs.est.7b05046.

Mahmoudi, N., Slater, G. F., and Fulthorpe, R. R. (2011). Comparison of commercial DNA extraction kits for isolation and purification of bacterial and eukaryotic DNA from PAH-

contaminated soils. *Canadian Journal of Microbiology* 57, 623–628. doi:10.1139/w11-049.

Markelova, E. (2017). Redox potential and mobility of contaminant oxyanions (As, Sb, Cr) in argillaceous rock subjected to oxic and anoxic cycles. PhD Thesis, University of Waterloo, Waterloo, Canada, 219 pp.

Martinez-Cruz, K., Leewis, M. C., Herriott, I. C., Sepulveda-Jauregui, A., Anthony, K. W., Thalasso, F., et al. (2017). Anaerobic oxidation of methane by aerobic methanotrophs in sub-Arctic lake sediments. *Science of the Total Environment* 607–608, 23–31. doi:10.1016/j.scitotenv.2017.06.187.

Milucka, J., Ferdelman, T. G., Polerecky, L., Franzke, D., Wegener, G., Schmid, M., et al. (2012). Zero-valent sulphur is a key intermediate in marine methane oxidation. *Nature* 491, 541–546. doi:10.1038/nature11656.

Misiti, T., Tandukar, M., Tezel, U., and Pavlostathis, S. G. (2013). Inhibition and biotransformation potential of naphthenic acids under different electron accepting conditions. *Water Research* 47, 406–418. doi:10.1016/j.watres.2012.10.019.

Mitterer, R. M. (2010). Methanogenesis and sulfate reduction in marine sediments: a new model. *Earth and Planetary Science Letters* 295, 358–366. doi:10.1016/j.epsl.2010.04.009.

Mohamad Shahimin, M. F., Foght, J. M., and Siddique, T. (2016). Preferential methanogenic biodegradation of short-chain n-alkanes by microbial communities from two different oil sands tailings ponds. *Science of the Total Environment* 553, 250–257. doi:10.1016/j.scitotenv.2016.02.061.

Nordstrom, D. K. (1977). Thermochemical redox equilibria of ZoBell's solution. *Geochimica et Cosmochimica Acta* 41, 1835–1841. doi:10.1016/0016-7037(77)90215-0.

Oswald, K., Milucka, J., Brand, A., Hach, P., Littmann, S., Wehrli, B., et al. (2016). Aerobic gammaproteobacterial methanotrophs mitigate methane emissions from oxic and anoxic lake waters. *Limnology and Oceanography* 61, S101–S118. doi:10.1002/lno.10312.

Parks, D. H., Chuvochina, M., Waite, D. W., Rinke, C., Skarshewski, A., Chaumeil, P. A., et al. (2018). A proposal for a standardized bacterial taxonomy based on genome phylogeny. *bioRxiv*, 1–35. doi:10.1101/256800.

Penner, T. J., and Foght, J. M. (2010). Mature fine tailings from oil sands processing harbour diverse methanogenic communities. *Canadian Journal of Microbiology* 56, 459–70. doi:10.1139/W10-029.

Plugge, C. M., Zhang, W., Scholten, J. C. M., and Stams, A. J. M. (2011). Metabolic flexibility of sulfate-reducing bacteria. *Frontiers in Microbiology* 2, 1–8. doi:10.3389/fmicb.2011.00081.

Poser, A., Lohmayer, R., Vogt, C., Knoeller, K., Planer-Friedrich, B., Sorokin, D., et al. (2013). Disproportionation of elemental sulfur by haloalkaliphilic bacteria from soda lakes. *Extremophiles* 17, 1003–1012. doi:10.1007/s00792-013-0582-0.

Postma, D., and Jakobsen, R. (1996). Redox zonation: Equilibrium constraints on the Fe(III)/SO4-reduction interface. *Geochimica et Cosmochimica Acta* 60, 3169–3175.

Ramos-Padrón, E., Bordenave, S., Lin, S., Bhaskar, I. M., Dong, X., Sensen, C. W., et al. (2011). Carbon and sulfur cycling by microbial communities in a gypsum-treated oil sands tailings pond. *Environmental Science and Technology* 45, 439–446. doi:10.1021/es1028487.

Reid, M. L., and Warren, L. A. (2016). S reactivity of an oil sands composite tailings deposit undergoing reclamation wetland construction. *Journal of Environmental Management* 166, 321–329. doi:10.1016/j.jenvman.2015.10.014.

Rios-Del Toro, E. E., Valenzuela, E. I., López-Lozano, N. E., Córtes-Martínez, M. G., Sánchez-Rodríguez, M. A., Calvario-Martínez, O., et al. (2018). Anaerobic ammonium oxidation linked to sulfate and ferric iron reduction fuels nitrogen loss in marine sediments. *Biodegradation*, 1-14. doi:10.1007/s10532-018-9839-8.

Risacher, F. F., Morris, P. K., Arriaga, D., Goad, C., Nelson, T. C., Slater, G. F., et al. (2018). The interplay of methane and ammonia as key oxygen consuming constituents in early stage development of Base Mine Lake, the first demonstration oil sands pit lake. *Applied Geochemistry* 93, 49–59. doi:10.1016/j.apgeochem.2018.03.013.

Rognes, T., Flouri, T., Nichols, B., Quince, C., and Mahé, F. (2016). VSEARCH: a versatile open source tool for metagenomics. *PeerJ* 4:e2584. doi:10.7717/peerj.2584.

Saidi-Mehrabad, A., He, Z., Tamas, I., Sharp, C. E., Brady, A. L., Rochman, F. F., et al. (2013). Methanotrophic bacteria in oil sands tailings ponds of northern Alberta. *The ISME Journal* 7,

908–21. doi:10.1038/ismej.2012.163.

Schloss, P. D., Westcott, S. L., Ryabin, T., Hall, J. R., Hartmann, M., Hollister, E. B., et al. (2009). Introducing mothur: open-source, platform-independent, community-supported software for describing and comparing microbial communities. *Applied and Environmental Microbiology* 75, 7537–7541. doi:10.1128/AEM.01541-09.

Schubert, C. J., Durisch-Kaiser, E., Wehrli, B., Thamdrup, B., Lam, P., and Kuypers, M. M. M. (2006). Anaerobic ammonium oxidation in a tropical freshwater system (Lake Tanganyika). *Environ Microbiol* 8, 1857–1863. doi:10.1111/j.1462-2920.2006.001074.x.

Siddique, T., Fedorak, P. M., and Foght, J. M. (2006). Biodegradation of short-chain n-alkanes in oil sands tailings under methanogenic conditions. *Environmental Science and Technology* 40, 5459–5464. doi:10.1021/es060993m.

Siddique, T., Fedorak, P. M., Mackinnon, M. D., and Foght, J. M. (2007). Metabolism of BTEX and naphtha compounds to methane in oil sands tailings. *Environmental Science and Technology* 41, 2350–2356. doi:10.1021/es062852q.

Siddique, T., Kuznetsov, P., Kuznetsova, A., Arkell, N., Young, R., Li, C., et al. (2014a). Microbially-accelerated consolidation of oil sands tailings. Pathway I: changes in porewater chemistry. *Frontiers in Microbiology* 5, 1–11. doi:10.3389/fmicb.2014.00106.

Siddique, T., Kuznetsov, P., Kuznetsova, A., Li, C., Young, R., Arocena, J. M., et al. (2014b). Microbially-accelerated consolidation of oil sands tailings. Pathway II: solid phase biogeochemistry. *Frontiers in Microbiology* 5, 1–15. doi:10.3389/fmicb.2014.00107.

Siddique, T., Penner, T., Klassen, J., Nesbø, C., and Foght, J. M. (2012). Microbial communities involved in methane production from hydrocarbons in oil sands tailings. *Environmental Science and Technology* 46, 9802–9810. doi:10.1021/es302202c.

Siddique, T., Penner, T., Semple, K., and Foght, J. M. (2011). Anaerobic biodegradation of longer-chain n-alkanes coupled to methane production in oil sands tailings. *Environmental Science and Technology* 45, 5892–5899. doi:10.1021/es200649t.

Sievert, S. M., Scott, K. M., Klotz, M. G., Chain, P. S. G., Hauser, L. J., Hemp, J., et al. (2008). Genome of the epsilonproteobacterial chemolithoautotroph Sulfurimonas denitrificans.

Applied and Environmental Microbiology 74, 1145–1156. doi:10.1128/AEM.01844-07.

Small, C. C., Cho, S., Hashisho, Z., and Ulrich, A. C. (2015). Emissions from oil sands tailings ponds: review of tailings pond parameters and emission estimates. *Journal of Petroleum Science and Engineering* 127, 490–501. doi:10.1016/j.petrol.2014.11.020.

Stasik, S., Loick, N., Knöller, K., Weisener, C., and Wendt-Potthoff, K. (2014). Understanding biogeochemical gradients of sulfur, iron and carbon in an oil sands tailings pond. *Chemical Geology* 382, 44–53. doi:10.1016/j.chemgeo.2014.05.026.

Stasik, S., and Wendt-Potthoff, K. (2014). Interaction of microbial sulphate reduction and methanogenesis in oil sands tailings ponds. *Chemosphere* 103, 59–66. doi:10.1016/j.chemosphere.2013.11.025.

Stasik, S., and Wendt-Potthoff, K. (2016). Vertical gradients in carbon flow and methane production in a sulfate-rich oil sands tailings pond. *Water Research* 106, 223–231. doi:10.1016/j.watres.2016.09.053.

Stoddard, S. F., Smith, B. J., Hein, R., Roller, B. R. K., and Schmidt, T. M. (2015). rrnDB: Improved tools for interpreting rRNA gene abundance in bacteria and archaea and a new foundation for future development. *Nucleic Acids Research* 43, D593–D598. doi:10.1093/nar/gku1201.

Tan, B., Charchuk, R., Li, C., Nesbo, C., Abu Laban, N., and Foght, J. (2014). Draft genome sequence of uncultivated Firmicutes (Peptococcaceae SCADC) single cells sorted from methanogenic alkane-degrading cultures. *Genome Announcements* 2, 1-2. doi:10.1128/genomeA.00909-14.

Walters, W., Hyde, E. R., Berg-Lyons, D., Ackermann, G., Humphrey, G., Parada, A., et al. (2015). Improved bacterial 16S rRNA gene (V4 and V4-5) and fungal internal transcribed spacer marker gene primers for microbial community surveys. *mSystems* 1, 1–10. doi:10.1128/ mSystems.00009-15.

Warren, L. A., Kendra, K. E., Brady, A. L., and Slater, G. F. (2016). Sulfur biogeochemistry of an oil sands composite tailings deposit. *Frontiers in Microbiology* 6, 1-14. doi:10.3389/fmicb.2015.01533.

Wenk, C. B., Blees, J., Zopfi, J., Veronesi, M., Bourbonnais, A., Schubert, C. J., et al. (2013). Anaerobic ammonium oxidation (anammox) bacteria and sulfide-dependent denitrifiers coexist in the water column of a meromictic south-alpine lake. *Limnology and Oceanography* 58, 1–12. doi:10.4319/lo.2013.58.1.0001.

White, K. B., and Liber, K. (2018). Early chemical and toxicological risk characterization of inorganic constituents in surface water from the Canadian oil sands first large-scale end pit lake. *Chemosphere* 211, 745–757. doi:10.1016/j.chemosphere.2018.07.059.

Yanagawa, K., Sunamura, M., Lever, M. A., Morono, Y., Hiruta, A., Ishizaki, O., et al. (2011). Niche separation of methanotrophic archaea (ANME-1 and -2) in methane-seep sediments of the Eastern Japan Sea offshore Joetsu. *Geomicrobiology Journal* 28, 118–129. doi:10.1080/01490451003709334.

Yue, J. C., and Clayton, M. K. (2005). A similarity measure based on species proportions. *Communications in Statistics - Theory and Methods* 34, 2123–2131. doi:10.1080/STA-200066418.

Zopfi, J., Ferdelman, T. G., and Fossing, H. (2004). Distribution and fate of sulfur intermediates - sulfite, tetrathionate, thiosulfate, and elemental sulfur - in marine sediments. *The Geological Society of America: Special Paper* 379, 97–116.

APPENDIX A: GEOCHEMISTRY

Table A-1: Eh values for the July 2017 sampling campaign. All values are in mV and corrected to the standard hydrogen electrode. All depths are in meters.

Platform	Depth Below Surface	Depth Below TWI	Eh
P1_07/17	9.6	-0.4	309
P1_07/17	9.7	-0.3	300
P1_07/17	9.8	-0.2	299
P1_07/17	9.9	-0.1	309
P1_07/17	10	0	299
P1_07/17	10.1	0.1	46
P1_07/17	10.2	0.2	-27
P1_07/17	10.3	0.3	13
P1_07/17	10.4	0.4	107
P1_07/17	10.5	0.5	215
P1_07/17	10.6	0.6	248
P1_07/17	10.7	0.7	239
P1_07/17	10.8	0.8	217
P1_07/17	10.9	0.9	269
P1_07/17	11	1	145
P1_07/17	11.1	1.1	273
P1_07/17	11.2	1.2	291
P1_07/17	11.3	1.3	113
P1_07/17	11.4	1.4	274
P1_07/17	11.5	1.5	232
P1_07/17	12	2	200
P1_07/17	12.5	2.5	108
P1_07/17	13	3	98
P1_07/17	14	4	129
P1_07/17	15	5	100
P1_07/17	16	6	86
P1_07/17	17	7	41
P1_07/17	18	8	134
P1_07/17	19	9	4
P1_07/17	20	10	35
P1_07/17	22	12	66
P1_07/17	24	14	95
P1_07/17	26	16	76
P1_07/17	28	18	77

Platform	Depth Below Surface	Depth Below TWI	Eh
P1_07/17	30	20	167
P1_07/17	34	24	163
P1_07/17	38	28	149
P1_07/17	42	32	182
P1_07/17	46	36	199
P1_07/17	50	40	301
P2_07/17	10.9	-0.75	348
P2_07/17	11	-0.65	361
P2_07/17	11.1	-0.55	349
P2_07/17	11.2	-0.45	346
P2_07/17	11.3	-0.35	346
P2_07/17	11.4	-0.25	351
P2_07/17	11.5	-0.15	337
P2_07/17	11.6	-0.05	340
P2_07/17	11.7	0.05	180
P2_07/17	11.8	0.15	-9
P2_07/17	11.9	0.25	51
P2_07/17	12	0.35	89
P2_07/17	12.1	0.45	42
P2_07/17	12.2	0.55	89
P2_07/17	12.3	0.65	108
P2_07/17	12.4	0.75	12
P2_07/17	12.5	0.85	126
P2_07/17	12.6	0.95	103
P2_07/17	12.7	1.05	82
P2_07/17	12.8	1.15	2
P2_07/17	12.9	1.25	212
P2_07/17	13.4	1.75	235
P2_07/17	13.9	2.25	182
P2_07/17	14.4	2.75	230
P2_07/17	15.4	3.75	110
P2_07/17	16.4	4.75	133
P2_07/17	17.4	5.75	170
P2_07/17	18.4	6.75	193
P2_07/17	19.4	7.75	203
P2_07/17	20.4	8.75	187
P2_07/17	21.4	9.75	136
P2_07/17	22.4	10.75	173
P2_07/17	23.4	11.75	140

Platform	Depth Below Surface	Depth Below TWI	Eh
P2_07/17	25.4	13.75	138
P2_07/17	27.4	15.75	90
P2_07/17	29.4	17.75	155
P3_07/17	9.1	-0.45	380
P3_07/17	9.3	-0.25	366
P3_07/17	9.4	-0.15	369
P3_07/17	9.5	-0.05	220
P3_07/17	9.6	0.05	23
P3_07/17	9.7	0.15	32
P3_07/17	9.8	0.25	193
P3_07/17	9.9	0.35	121
P3_07/17	10	0.45	310
P3_07/17	10.1	0.55	221
P3_07/17	10.2	0.65	194
P3_07/17	10.3	0.75	165
P3_07/17	10.4	0.85	165
P3_07/17	10.5	0.95	228
P3_07/17	10.7	1.15	240
P3_07/17	11	1.45	188
P3_07/17	11.5	1.95	245
P3_07/17	12	2.45	178
P3_07/17	12.5	2.95	230
P3_07/17	13.5	3.95	45
P3_07/17	14.5	4.95	140
P3_07/17	15.5	5.95	174
P3_07/17	16.5	6.95	164
P3_07/17	17.5	7.95	111
P3_07/17	18.5	8.95	190
P3_07/17	19.5	9.95	0
P3_07/17	21.5	11.95	40
P3_07/17	23.5	13.95	153
P3_07/17	25.5	15.95	64
P3_07/17	27.5	17.95	186
P3_07/17	29.5	19.95	75
P3_07/17	33.5	23.95	189
P3_07/17	37.5	27.95	102
P3_07/17	41.5	31.95	137
P3_07/17	42.9	33.35	142

APPENDIX B: MICROBIOLOGY

Table B-1: Samples collected for microbiological analysis and their corresponding DNA concentrations. Letters and associated values represent triplicate DNA extractions. All depths are in meters and DNA concentrations are in ng μL^{-1}.

Sample Location/Time	Depth Below Water Surface	Depth Below TWI	DNA Concentration
P1_08/16	9.5	0.05	A: 1.57 B: 1.93 C: 1.75
P1_08/16	9.6	0.15	A: 0.097 B: 0.092 C: 0.111
P1_08/16	9.8	0.35	A: 0.192 B: 0.107 C: 0.240
P1_08/16	10.5	1.05	A: 0.256 B: 0.075 C: 0.332
P1_08/16	11.5	2.05	A: 0.156 B: 0.127 C: 0.024
P1_08/16	12.5	3.05	A: 0.037 B: 0.195 C: 0.181
P1_08/16	14.0	4.55	A: 0.012 B: 0.006 C: 0.007
P1_08/16	16.0	6.55	A: 0.107 B: 0.144 C: 0.028
P1_08/16	20.0	10.55	A: 0.023 B: 0.017 C: 0.011
P2_08/16	11.2	0.05	A: 3.50 B: 3.24 C: 3.56
P2_08/16	11.3	0.15	A: 1.63 B: 1.47 C: 1.34
P2_08/16	11.4	0.25	A: 0.452 B: 0.232 C: 0.538

Sample Location/Time	Depth Below Water Surface	Depth Below TWI	DNA Concentration
P2_08/16	11.9	0.75	A: 0.185 B: 0.114 C: 0.242
P2_08/16	12.5	1.35	A: 0.220 B: 0.260 C: 0.382
P2_08/16	14.0	2.85	A: 0.063 B: 0.042 C: 0.034
P2_08/16	17.0	5.85	A: 0.105 B: 0.140 C: 0.110
P2_08/16	21.0	9.85	A: 0.055 B: 0.085 C: 0.059
P3_08/16	9.3	0.00	A: 2.26 B: 2.10 C: 2.36
P3_08/16	9.4	0.10	A: 1.24 B: 1.05 C: 1.24
P3_08/16	9.6	0.30	A: 0.714 B: 0.744 C: 0.722
P3_08/16	9.8	0.50	A: 0.141 B: 0.129 C: 0.111
P3_08/16	10.3	1.0	A: 0.113 B: 0.112 C: 0.101
P3_08/16	11.3	2.0	A: 0.070 B: 0.062 C: 0.100
P3_08/16	14.0	4.7	A: 0.111 B: 0.096 C: 0.140
P3_08/16	17.0	7.7	A: 0.226 B: 0.189 C: 0.173
P3_08/16	20.0	9.7	A: 0.060 B: 0.070 C: 0.100

Sample Location/Time	Depth Below Water Surface	Depth Below TWI	DNA Concentration
P1_03/17	9.65	0.05	A: 9.84 B: 11.2 C: 10.2
P1_03/17	9.85	0.25	A: 6.68 B: 5.50 C: 5.56
P1_03/17	9.95	0.35	A: 2.22 B: 2.20 C: 2.52
P1_03/17	11.05	1.45	A: 0.616 B: 0.580 C: 0.578
P2_03/17	9.75	0.05	A: 21.6 B: 16.2 C: 18.3
P2_03/17	9.85	0.15	A: 4.50 B: 3.68 C: 3.32
P2_03/17	10.05	0.35	A: 0.524 B: 0.412 C: 0.528
P2_03/17	11.15	1.45	A: 0.676 B: 0.680 C: 0.952
P3_03/17	8.85	0.05	A: 1.70 B: 1.88 C: 1.77
P3_03/17	8.95	0.15	A: 0.998 B: 0.694 C: 1.05
P3_03/17	9.15	0.35	A: 0.568 B: 0.634 C: 0.498
P3_03/17	10.15	1.35	A: 0.532 B: 0.676 C: 0.794
P1_07/17	10.1	0.10	A: 7.58 B: 8.72 C: 6.36
P1_07/17	10.2	0.20	A: 4.02 B: 4.24 C: 4.14

Sample Location/Time	Depth Below Water Surface	Depth Below TWI	DNA Concentration
P1_07/17	11.0	1.0	A: 0.976 B: 1.23 C: 1.09
P1_07/17	15.0	5.0	A: 0.206 B: 0.242 C: 0.216
P1_07/17	20.0	10.0	A: 0.184 B: 0.181 C: 0.216
P1_07/17	30.0	20.0	A: 0.206 B: 0.186 C: 0.25
P1_07/17	42.0	32.0	A: 0.119 B: 0.094 C: 0.102
P2_07/17	11.7	0.05	A: 2.88 B: 2.96 C: 2.80
P2_07/17	11.8	0.15	A: 1.13 B: 1.27 C: 1.36
P2_07/17	12.6	0.95	A: 0.658 B: 0.498 C: 0.598
P2_07/17	16.4	4.75	A: 0.380 B: 0.350 C: 0.532
P2_07/17	21.4	9.75	A: 0.228 B: 0.226 C: 0.334
P2_07/17	25.4	13.75	A: 0.268 B: 0.300 C: 0.354
P2_07/17	29.4	17.75	A: 0.230 B: 0.190 C: 0.388
P3_07/17	9.6	0.05	A: 13.7 B: 13.8 C: 8.98
P3_07/17	9.7	0.15	A: 3.46 B: 3.51 C: 2.04

Sample Location/Time	Depth Below Water Surface	Depth Below TWI	DNA Concentration
P3_07/17	10.5	0.95	A: 0.911 B: 0.849 C: 1.10
P3_07/17	14.5	4.95	A: 0.083 B: 0.099 C: 0.102
P3_07/17	19.5	9.95	A: 0.854 B: 0.640 C: 0.834
P3_07/17	29.5	19.95	A: 0.020 B: 0.013 C: 0.016
P3_07/17	42.9	33.35	A: 0.226 B: 0.144 C: 0.107

Table B-2: Summary table of alpha diversity calculations for all high-throughput amplicon samples. All samples were subsampled to 34 200 reads prior to calculations.

Sample Location/ Time	Depth Below TWI (m)	Good's Coverage	Observed OTUs (97% identity)	Inverse Simpson Index	Shannon Index	Chao Estimator	Ace Estimator
P1_08/16	0.05	0.980	1660	80.6	5.4	2683	3251
P1_08/16	0.15	0.985	1469	71.8	5.3	2070	2327
P1_08/16	0.35	0.985	1399	41.6	5.0	2032	2331
P1_08/16	1.05	0.986	1334	53.5	5.1	1931	2077
P1_08/16	2.05	0.987	1271	51.4	5.0	1750	1775
P1_08/16	3.05	0.988	1246	43.7	5.0	1744	1840
P1_08/16	4.55	0.996	899	68.8	5.1	989	982

Sample Location/ Time	Depth Below TWI (m)	Good's Coverage	Observed OTUs (97% identity)	Inverse Simpson Index	Shannon Index	Chao Estimator	Ace Estimator
P1_08/16	6.55	0.991	1073	57.0	5.0	1429	1423
P1_08/16	10.55	0.993	1030	51.6	5.0	1231	1229
P2_08/16	0.05	0.981	1557	64.9	5.2	2568	3121
P2_08/16	0.15	0.981	1578	66.8	5.3	2557	3109
P2_08/16	0.25	0.981	1612	68.4	5.3	2584	3184
P2_08/16	0.75	0.985	1318	43.2	5.0	1999	2432
P2_08/16	1.35	0.986	1322	54.6	5.1	1991	2268
P2_08/16	2.85	0.991	1043	33.5	4.6	1359	1370
P2_08/16	5.85	0.989	994	21.1	4.3	1492	1824
P2_08/16	9.85	0.990	927	18.4	4.2	1329	1362
P3_08/16	0.00	0.977	1830	91.2	5.5	3058	3755
P3_08/16	0.10	0.978	1817	90.4	5.5	2955	3595
P3_08/16	0.30	0.981	1604	78.6	5.4	2583	3078
P3_08/16	0.50	0.984	1464	62.8	5.2	2143	2480
P3_08/16	1.0	0.985	1366	45.9	5.0	2044	2443
P3_08/16	2.0	0.987	1281	44.9	5.0	1769	1795

Sample Location/ Time	Depth Below TWI (m)	Good's Coverage	Observed OTUs (97% identity)	Inverse Simpson Index	Shannon Index	Chao Estimator	Ace Estimator
P3_08/16	4.7	0.988	1142	32.1	4.7	1686	2023
P3_08/16	7.7	0.987	1224	70.4	5.2	1753	2078
P3_08/16	9.7	0.988	1195	58.4	5.0	1657	1781
P1_03/17	0.05	0.979	1705	36.2	5.2	2798	3478
P1_03/17	0.25	0.980	1697	77.0	5.5	2785	3423
P1_03/17	0.35	0.980	1687	92.2	5.6	2750	3346
P1_03/17	1.45	0.984	1424	58.1	5.2	2236	2626
P2_03/17	0.05	0.979	1762	53.5	5.4	2850	3355
P2_03/17	0.15	0.979	1728	99.8	5.6	2814	3476
P2_03/17	0.35	0.983	1470	53.8	5.1	2285	2747
P2_03/17	1.45	0.984	1353	46.7	5.0	2183	2666
P3_03/17	0.05	0.985	1302	35.2	4.8	2100	2564
P3_03/17	0.15	0.985	1243	32.3	4.7	1988	2383
P3_03/17	0.35	0.983	1464	42.5	5.0	2338	2775
P3_03/17	1.35	0.985	1260	33.7	4.8	1986	2486
P1_07/17	0.10	0.977	1891	74.5	5.5	3080	3749

Sample Location/ Time	Depth Below TWI (m)	Good's Coverage	Observed OTUs (97% identity)	Inverse Simpson Index	Shannon Index	Chao Estimator	Ace Estimator
P1_07/17	0.20	0.979	1741	90.0	5.6	2909	3659
P1_07/17	1.0	0.984	1395	55.6	5.1	2227	2614
P1_07/17	5.0	0.985	1287	63.1	5.1	2016	2431
P1_07/17	10.0	0.988	1175	45.7	4.9	1611	1650
P1_07/17	20.0	0.986	1123	25.4	4.3	1789	2241
P1_07/17	32.0	0.988	1030	27.4	4.4	1526	1777
P2_07/17	0.05	0.980	1603	55.4	5.2	2658	3265
P2_07/17	0.15	0.983	1383	30.3	4.8	2220	2673
P2_07/17	0.95	0.983	1415	31.7	4.9	2195	2631
P2_07/17	4.75	0.987	1101	16.7	4.4	1692	2064
P2_07/17	9.75	0.986	1180	22.3	4.5	1843	2264
P2_07/17	13.75	0.984	1312	28.7	4.6	2138	2775
P2_07/17	17.75	0.986	1124	14.1	4.1	1872	2355
P3_07/17	0.05	0.976	1912	69.5	5.5	3221	3994
P3_07/17	0.15	0.980	1681	75.4	5.4	2709	3375
P3_07/17	0.95	0.983	1482	57.0	5.1	2387	2876

Sample Location/ Time	Depth Below TWI (m)	Good's Coverage	Observed OTUs (97% identity)	Inverse Simpson Index	Shannon Index	Chao Estimator	Ace Estimator
P3_07/17	4.95	0.987	1256	41.8	4.9	1760	1811
P3_07/17	9.95	0.985	1265	48.1	5.0	2049	2500
P3_07/17	19.95	0.993	998	40.2	4.9	1191	1181
P3_07/17	33.35	0.988	1114	39.9	4.7	1638	1999

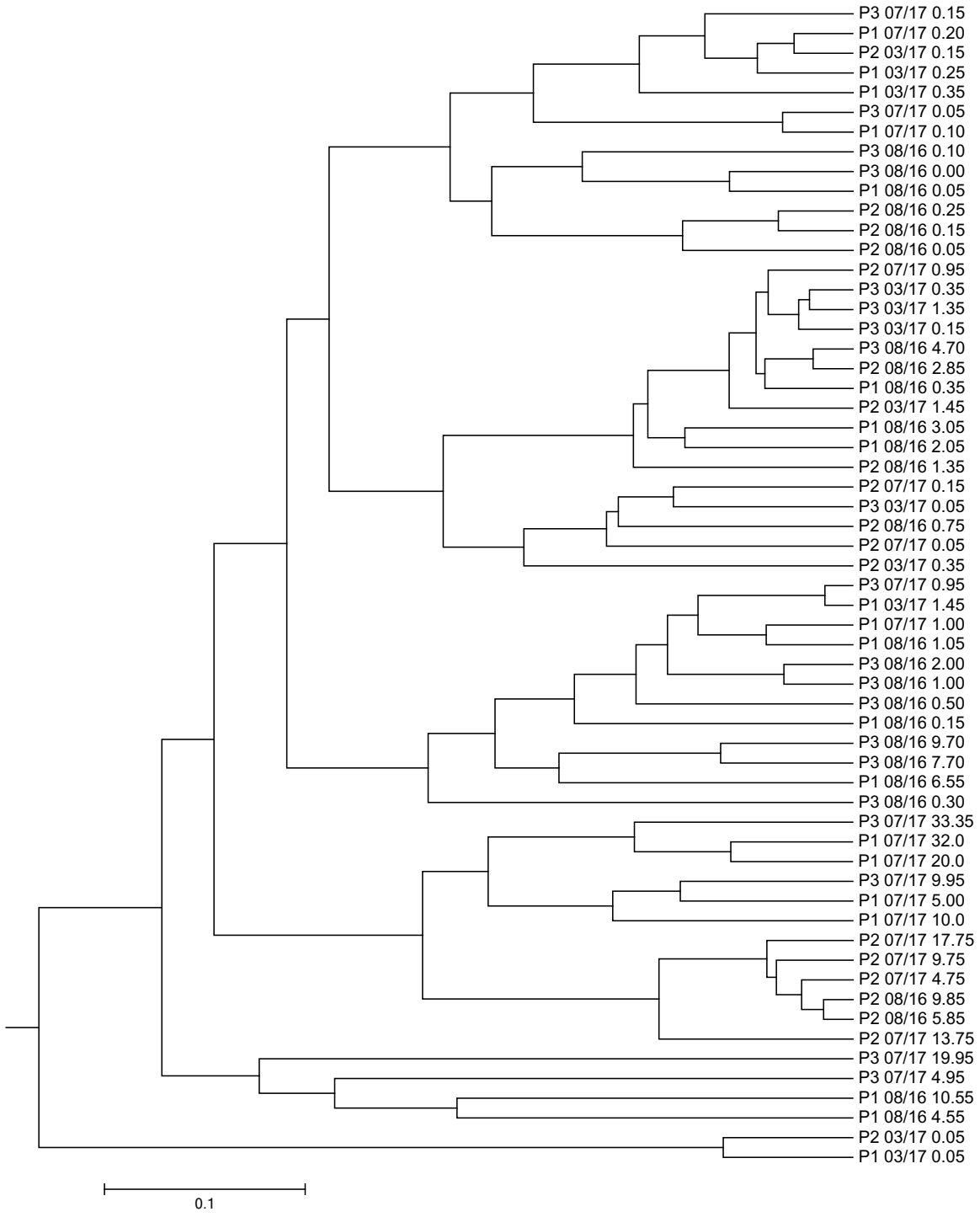

Figure B-1: Dendrogram created using the theta Yue-Clayton index. The labelling is depicted as the platform location, followed by the date of sample collection and the depth below the TWI in meters.

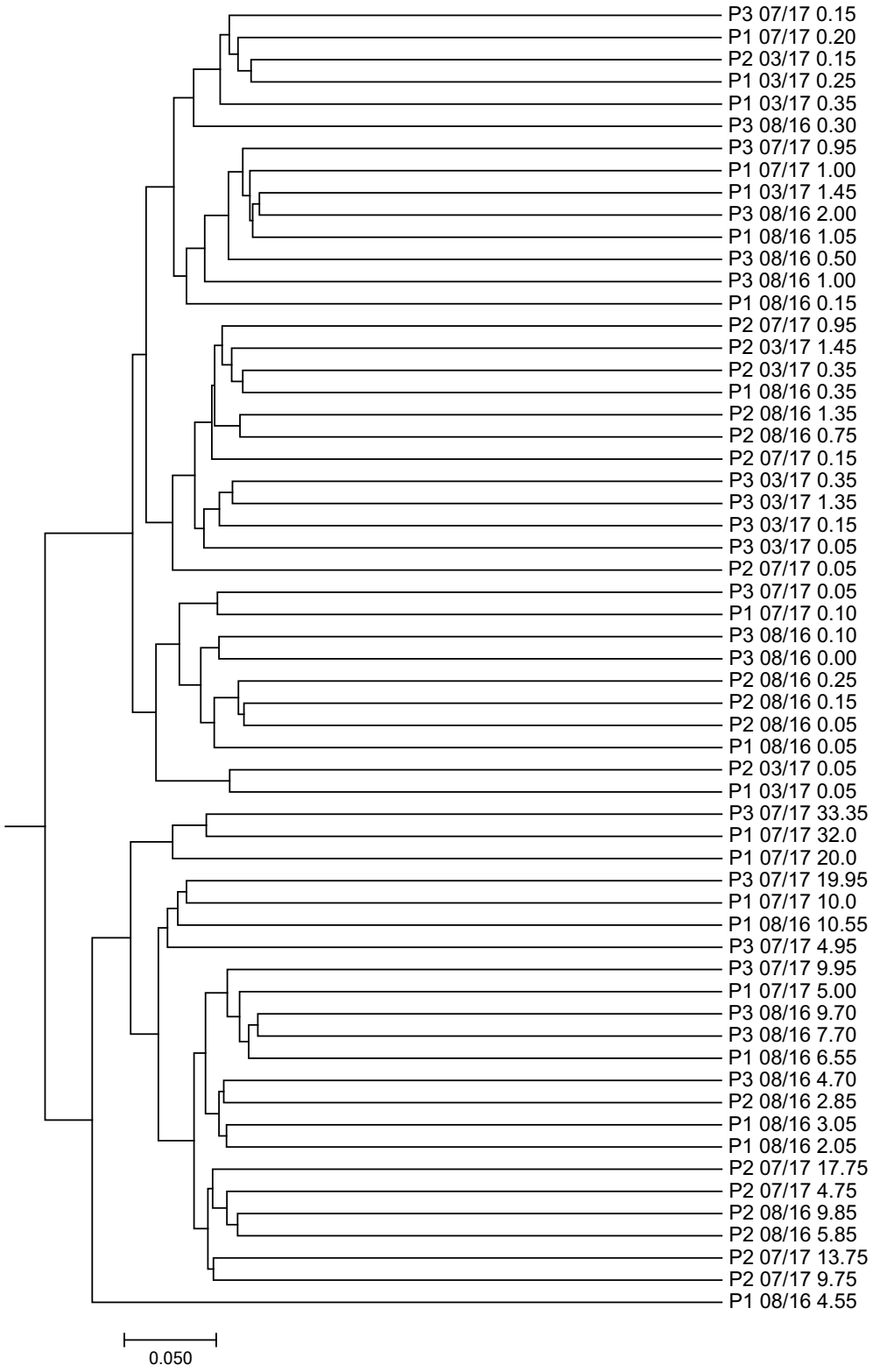

Figure B-2: Dendrogram created using the Jaccard index. The labelling is depicted as the platform location, followed by the date of sample collection and the depth below the TWI in meters.